Study on the measurement of phase distribution of vortex beams by sinusoidal phase modulation method

Doctoral Program of Electrical and Information Engineering
Graduate School of Science and Technology
Niigata University

PU HAOSEN

February 2023

Abstract

The vortex beam (VB) with a helix wavefront has a wide range of applications in optical manipulation and information processing. In the past decades, some research on the vortex phenomenon had remarkable development and the research on VB has gradually become an important branch of modern optics. The spiral wavefront of VB is characterized by characteristics phase of $\exp(il\theta)$ with the topological charge of l and the azimuth angle of θ. The unique spiral phase structure presents a hollow bright ring in the intensity distribution of VB and yields a phase singularity in the optical axis with the undefine phase and amplitude of zero. Because of the helix wavefront, each photon of VB possesses the orbital angular momentum (OAM), given by $\hbar l$,related to the topological charge, where the $\hbar$ is the Planck constant. Considering the unique property of OAM, the VB has a wide range of applications in optical tweezers and information processing. For example, the focused VB generating the electric field gradient force can be used for capturing particle, making it rotate around the optical axis of VB. In addition, the property of OAM can be used for fabricating the chiral micro-scale structures materials as well. In the optical communication field, the OAM can have been used as an alternative degree of freedom for multiplexing modulation, thereby enlarging the capacity of optical communication, which is also referred to as mode/spatial-division multiplexing. Given these applications using the feature of the VB, the phase distribution of a wavefront of VB, which is related to the topological charge, is the one of most crucial parameters.

Therefore, investigation of the property of VB and proposing the phase measurement method of VB are significant for these applications using the VB.

Main research and innovations of this thesis are as follows:

(1) Investigation of the property of vortex beam.

The VB with the spiral phase structure is derived from wave equation under the condition paraxial approximation. Due to the spiral wavefront, each photon of VB possessing the OAM that has many applications in optical tweezers and optical communication. In the experiment, the common VB has mainly two types for Laguerre-Gaussian and Bessel beams. Considering these applications, the generation of high quality of VB is essential and the general methods of generating VB is mainly classified to Laser mode modulation and phase element.

(2) Sinusoidal phase modulation method

Phase measurement of the VB as well as estimation of the topological charge are significant for these applications. Some methods of phase measurement of VB have been proposed. Nevertheless, these methods have some obvious disadvantage due to the complex experimental configuration and data processing. Therefore, the Sinusoidal phase modulation method is proposed to measure the phase profile of vortex wavefront based the interferometric measurement technique with the high measurement accuracy and the simple data processing method. Due to more convenient configuration and straightforward calibration, the SPM is excellent method for phase measurement of VB.

(3) Estimation method of topological charge

The topological charge of VB is the one of most crucial parameters as well and defined by the maximum variation in phase distribution of the VB along to the azimuth angle. Hence, the continuous variation of phase along to azimuth angle in wrapped phase was

used for estimating the topological charge. However, due to the discontinuous phase distribution in wrapped phase distribution of VB, it may lead to the enormous measurement error. For obtaining the continuous phase distribution of VB, the phase unwrapping method based on polar coordinates used for estimating the topological charge can distinguish the position of phase singularity and phase step, with high measurement accuracy.

(4) Reduction of effect of phase singularity

The phase singularity with an undefined phase and amplitude of zero must be reduced or eliminated in advance. Because of the intensity in the position of phase singularity being far small from other pixel of intensity of VB, the suitable threshold value of measured intensity of VB was defined to reduce the part of phase singularity only that the above the threshold value of intensity is highlighted.

CONTENT

1. Introduction

1.1 Overview

The abnormal light spot with a bright ring was accidentally discovered on the focal plane of a lens by Airy in the 1830s [1, 2], which prompted many researchers to analyze the vortex phenomenon from the view of optics. The earliest research on the vortex beam (VB) can be dated from the 1930s [3]. In 1974, Nye and Berry studied the property of phase singularity and introduced the concept of phase isolation with an undefined phase into the center of a light beam [4]. The wave equation of the VB yields a phase singularity in the position of the modulus of zero and the corresponding amplitude of zero. The view of vortex not only was discovered in the optical fields but also considered to describe the movement of micro-particle [5]. In 1989, the concept of the ideal optical vortex with a spiral phase structure was the first time to be proposed by Coullet via the solution of Maxwell Bloch equation [6]. The intensity distribution of VB is affected by the property of a phase singularity, which results in a hollow bright ring with a center dark space, which was shown in Fig.1.1(b). With the development of research on phase singularity and the property of OAM, the study on the VB and its applications have gradually become an important branch of modern optics [7].

The vortex wavefront in free space propagation is characterized by the spiral phase, which is shown in Fig.1.1(a), where the center position of wavefront is the phase singularity with an undefined phase. Moreover, the module of optical fields of VB in phase singularity is zero (Re(E)=Im(E)=0). The unique helix wavefront leads to each photon of VB possessing the OAM. Thereby, the focused VB can generate the gradient

force of electric field, which is similar to the optical tweezers, making a particle rotate around the optical axis of VB [8]. Moreover, the VB can be used for capturing the low refractive index of particle due to the dark space in the center of VB [9]. Simpson proved that the VB with the topological charge of l=1 is equivalence to the circularly polarized light in capturing the particle [10]. Further study indicates the OAM and the spin angular momentum (SAM) can be transformed each other under the specific condition [11]. In the optical communication field, the VB has been employed in atmospheric transmission because of the property of OAM with high stability during the process of propagation in turbulence [12]. Additionally, the VB can be used for storing information due to the high stability and security [13]. For the information encoding and decoding communication, the OAM as an alternative degree of freedom has been employed in communication carriers [14]. Further research on the encoding and decoding method reveals that the optical communication with the VB has a significant progress in the enhancements of communication capacity and the effective propagation distance [14-16]. By the space division multiplex for the OAM, the capacity of communication has broken through the magnitude of the units of Tbits [15]. Additionally, the VB has many significant applications in super-solution image [17] and optical manufacture [18], and so on. Considering these applications using these properties of VB, it reveals that the VB has a huge development in life science and optical communication fields.

Given that these applications, the phase distribution of VB, which is related to the topological charge, is the one of most crucial parameters. Therefore, the accurate measurements of the phase profiles of the wavefronts of VBs and estimation of the topological charge are required to guarantee the beam quality and improve the development efficiency of application. The diffraction and interference patterns of VB

depended on the property of topological charge, has been employed in estimating the topological charge [19-21]. However, these methods had an obvious disadvantage due to the uncertain phase information. Recently, the phase sensitive interferometry has been proposed for phase measurement of VB due to the high measurement accuracy and sensitive. For example, the four-step phase algorithm [22] and the heterodyne interferometry [23] have been employed in phase measurement of VB. Nevertheless, these methods had some obvious disadvantages due to the complex experimental configuration and data processing. In this thesis, a sinusoidal phase modulation method was used for achieving the vortex phase measurement purpose [24]. Comparing these methods, the SPM methods has more convenient configuration and straightforward calibration.

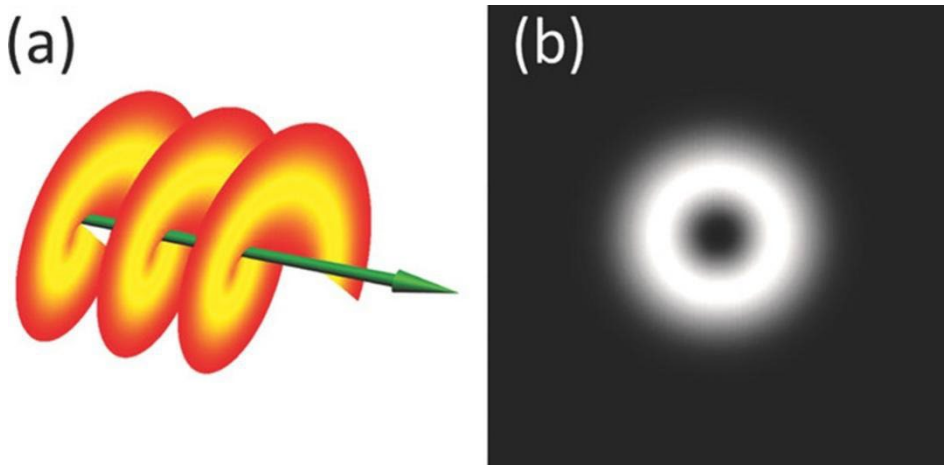

Fig.1.1 Intensity distribution of vortex beam and the diagram of vortex wavefront[25].

1.2 Principles of light with angular momentum

1.2.1 Solutions to the paraxial wave equation

In a source free space electromagnetic radiation is described by Maxwell's equations, and the wave equation can be solved under the condition of paraxial approximation by the Helmholtz equation. The scalar Helmholtz equation is represented as follows [26]:

$$(\nabla^2 + k^2)E = 0 \tag{1.1}$$

Where the k=2π/λ is the wave number. Under the condition of Cartesian coordinates, the general solution of the electric field for equation (1.1) is deduced

$$E(x,t,z,t) = u(x,y,z)\exp[(i(kz-\omega t))] \tag{1.2}$$

Using the slowly varying envelope approximation of and the variable's separation of x and y, the solution of Hermite-Gauss mode is obtained as follows

$$u(x,y,z) = E_0 H_m(\sqrt{2}\frac{x}{w(z)})H_n(\sqrt{2}\frac{y}{w(z)})\frac{w_0}{w(z)}\exp[-i\varphi_{mn}(z)]\exp[i\frac{k}{2q(z)}r^2] \tag{1.3}$$

where the $H_m(x)$ represents the Hermite polynomials, satisfying the following differential equation.

$$\frac{d^2H_m}{dx^2} - 2x\frac{dH_m}{dx} + 2mH_m = 0 \tag{1.4}$$

In Eq. (1.3), the E_0 indicates the amplitude constants of the electric field. The $w(z)$ and w_0 are the sizes of the light beam at the propagation distance of z and the waist radius, respectively. Moreover, the Rayleigh length is given by the $z_0=\pi w^2/\lambda$. $\varphi_{mn}(z) = (m+n+1)\tan^{-1}(z/z_0)$ is the Gouy phase and $q(z)$ is given by the $q(z)=z-iz_0$. Figure.1.2 shows the intensity distribution of the Hermite-Gauss beam generated by the numerical simulation. When the $m=n=0$, Eq. (1.3) can be simplified to be the solution of the Gaussian mode as follows.

$$u(r,z) = E_0\frac{w_0}{w(z)}\exp[-i\varphi(z)]\exp[i\frac{k}{2q(z)}r^2] \tag{1.5}$$

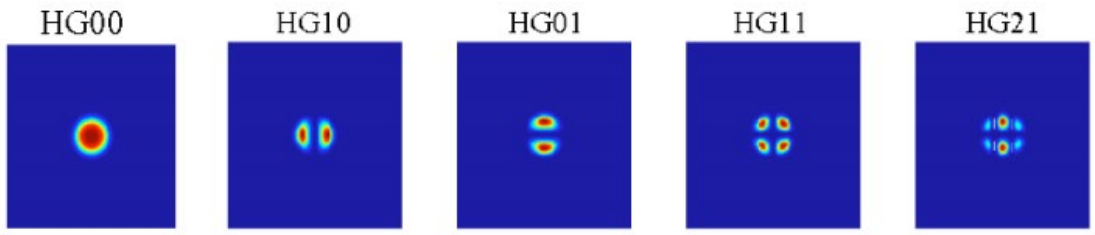

Fig.1.2 Intensity distribution of Hermite-Gauss beam [27].

where the $\varphi(z) = \tan^{-1}(z / z_0)$ is the simplified Gouy phase. Under the condition of cylindrical coordinates, the scalar general solution of the Helmholtz equation for Eq. (1.5) can be represented by

$$E(r,\phi,z,t) = u(r,\phi,z)\exp[i(kz-\omega t)] \tag{1.6}$$

Substituting Eq. (1.6) into Eq. (1.1) and using the slow varying envelop approximation as well, the following equation is obtained as

$$\frac{1}{r}\frac{\partial}{\partial r}(r\frac{\partial u}{\partial r})+\frac{1}{\mathrm{r}^2}\frac{\partial^2 u}{\partial \phi^2}+2ik\frac{\partial u}{\partial z}=0 \tag{1.7}$$

By means of the variable's separation, the solution of the Laguerre-Gauss mode is deduced as [28]

$$u(r,\phi,z) = E_0(\sqrt{2}\frac{r}{\omega})^l L_p^l(2\frac{r^2}{\omega^2})\frac{w_0}{w(z)}\exp[-i\phi_{pl}(z)]\exp[i\frac{k}{2q(z)}r^2]\exp(il\phi) \tag{1.8}$$

where the L_p^l is Laguerre polynomials. The l and p are the topological charge and the radial index respectively. Eq. (1.8) manifests that the LG beam has a vortex wavefront due to have an item of a spiral phase of $\exp(il\phi)$.

1.2.2 Vortex phase gradient theory

The complex amplitude of VB can be defined by [29]

$$\begin{aligned} E(x,y) &= (x+iy)^l = r^l \exp[i\varphi(x,y)] \\ \varphi &= l\theta = \arg[(x+iy)^l] \end{aligned} \tag{1.9}$$

Where the *r* represents the radial component in the cylindrical coordinates. Under the condition of polar coordinates, the phase gradient of VB can be represented by

$$\nabla\varphi = (\nabla\varphi)_r r + (\nabla\varphi)_\theta \theta$$

$$(\nabla\varphi)_r = \frac{\partial\varphi}{\partial r} \tag{1.10}$$

$$(\nabla\varphi)_\theta = \frac{1}{r}\frac{\partial\varphi}{\partial\theta} \tag{1.11}$$

where the $(\nabla\varphi)_r$ and $(\nabla\varphi)_\theta$ are the components of phase gradient in transverse and longitudinal direction respectively. The longitudinal component of phase gradient can be ignored in the calculation processing of phase gradient in transverse components. According to Eq. (1.9) and Eq. (1.10), the transverse component of the phase gradient can be obtained as follows.

$$\begin{aligned} (\nabla\varphi) &= 0 \\ (\nabla\varphi)_\theta &= \frac{l}{r} \end{aligned} \tag{1.12}$$

When the value of $\frac{\partial\varphi}{\partial\theta}$ is constants, the VB is isotropy, otherwise the VB is anisotropy due to the value of $\frac{\partial\varphi}{\partial\theta}$ is arbitrarily. Moreover, when the value of $\frac{\partial\varphi}{\partial\theta}$ is zero, the spiral wavefront disappears to be transformed the plane wavefront

When the value of $\frac{\partial\varphi}{\partial\theta}$ is constants, the state of isotropy for VB can be described by the line integral, as follows.

$$\oint \nabla\varphi ds = \int_0^{2\pi} \frac{l}{r}\theta \bullet r d\theta = 2\pi l \tag{1.13}$$

The optical field of VB with the state of anisotropy can be described by the Eq. (1,9) and

the corresponding phase distribution function can be represented by

$$\varphi(x,y) = l\arctan(\sigma\frac{x}{y}) = l\arctan(\sigma\frac{\sin\theta}{\cos\theta}) \tag{1.14}$$

where the σ is anisotropy parameters. According to the Eq. (1.14), the following equation is obtained as

$$\frac{\partial\varphi}{\partial\theta} = \frac{l\sigma}{\cos^2\theta + \sigma^2\sin^2\theta} \tag{1.15}$$

We introduce the trigonometric identity, represented by the Eq. (1.16)

$$\int\frac{d\theta}{A\sin^2\theta + B\cos^2\theta} = \frac{1}{\sqrt{AB}}\arctan(\sqrt{\frac{A}{B}}\tan\theta) + C \tag{1.16}$$

According to the Eq. (1.16), the anisotropy state can be described by

$$\int_0^{2\pi}\frac{1}{r}\frac{la}{\sin^2\theta + a^2\cos^2\theta}\cdot\theta\cdot rd\theta\cdot\theta = 2\pi l \tag{1.17}$$

In conclusion, the phase of VB around the center of optical axis and the phase gradient are always the integral multiple of 2π in the any situation . Therefore, the VB possesses a spiral phase structure and the property of OAM.

1.2.3 Basic theory of orbital angular momentum

The angular momentum (AM) is the inherent attribute of photon and the one of the crucial physical quantities. The normal photon of light beam possesses the spin angular momentum (SAM). Different from the normal light beam, the VB possesses the orbital angular momentum (OAM) [30], due to the vortex wavefront. Based on the classical electromagnetic theory, the concept of OAM is introduced in next section.

The angular momentum density of the optical field is given by the following equation, where the *E* and *B* are the electric field intensity and the magnetic field respectively

$$M = \varepsilon_0 \, r \times (E \times B) \tag{1.18}$$

where the ε_0 and r are the dielectric constant and the radial vector. Hence, the total angular momentum can be expressed by

$$J = \varepsilon_0 \int r \times (E \times B) d\, r \tag{1.19}$$

Obviously, the J indicates the total angular momentum of VB containing with the SAM of S and the OAM of L, given by $J=L+S$.

Under the condition of paraxial approximation, the electric field vectorial-potential in the x-axis component is given by A where the $E(x,y,z)$ denotes the complex amplitude of electric field .By the Lorentz gauge, the corresponding vector-potential of A can be represented by

$$A = xE(x, y, z)e^{ikz} \tag{1.20}$$

Moreover, the electric field intensity E and the magnetic field B for VB is expressed by

$$E = ik[Ee_x + \frac{i}{k}\frac{\partial E}{\partial y}e_z]e^{ikz} \tag{1.21}$$

$$B = \mu_0 H = ik[Ee_y + \frac{i}{k}\frac{\partial E}{\partial y}e_z]e^{-ikz} \tag{1.22}$$

According to the Eq. (1.10), the linear momentum density of light beam is deduced

$$\begin{aligned} &\varepsilon_0 \langle E \times B \rangle = i\omega \frac{1}{2}\varepsilon_0 (E\nabla E^* - E^* \nabla E) + \omega k \varepsilon_0 \\ &\omega = 2\pi\nu \end{aligned} \tag{1.23}$$

where the E^*, ω, and ν are the conjugate complex amplitude, angular frequency, and frequency respectively. Because of the OAM related to the component of linear momentum, the OAM density in z-axis can deduce

$$\begin{aligned} &J_z = (r \times \varepsilon_0 \langle E \times B \rangle)_z = r \cdot p_\theta \\ &p_\theta = \varepsilon_0 \langle E \times B \rangle_\theta \end{aligned} \tag{1.24}$$

where the p_θ indicates the component θ of the linear momentum. The complex amplitude of the optical field of the VB under the cylindrical coordinate can be expressed by

$$E(r,\theta,z) = E_0(r,z)e^{il\theta} \tag{1.25}$$

Using Eq. (1.23) and Eq. (1.25), the component of p_θ is obtained as

$$p_\theta = [i\omega\frac{1}{2}\varepsilon_0(E\nabla E^* - E^*\nabla E) + \omega k\varepsilon_0) = \frac{\omega\varepsilon_0\left|E\right|^2}{r} \tag{1.26}$$

According to Eq. (1.24) and Eq. (1.26), the OAM density in the z-axis is represented by

$$J_z = r\cdot p_\theta = \omega\varepsilon_0 l\left|E\right|^2 \tag{1.27}$$

Moreover, the energy flux density in z-axis direction is given by

$$s = cp_z = c\varepsilon_0\left\langle E\times B\right\rangle_z = \omega^2\varepsilon_0\left|E\right|^2 \tag{1.28}$$

where the c represents the velocity of light in vacuum. By means of the surface integral for the OAM and the energy flux density at the same cross section, their specific value can be deduced

$$\frac{J_z}{s} = \frac{\iint_{\Sigma_0} rdrd\theta(r\times\left\langle E\times B\right\rangle_z)}{c\iint_{\Sigma_0} rdrd\theta(\left\langle E\times B\right\rangle_z)} = \frac{l}{\omega} \tag{1.29}$$

Additionally, Using the Eq. (1.27) and Eq. (1.28), the specific value of OAM density and the energy flux density can be written as

$$\frac{J_z}{s} = \frac{l}{\omega} = \frac{l\hbar}{\omega\hbar} \tag{1.30}$$

Substituting the ω from the Eq. (1.23), into the Eq. (1.30), the following equation is deduced

$$\frac{l}{\omega} = \frac{l\hbar}{\omega\hbar} = \frac{l\hbar}{2\pi v\cdot\frac{h}{2\pi}} = \frac{l\hbar}{hv} \tag{1.31}$$

Therefore

$$\frac{J_z}{s} = \frac{l\hbar}{h\nu} \tag{1.32}$$

Hence, each photon energy of the VB is given by the *hv,* and possesses the OAM of $l\hbar$ for each photon of the VB, where the h and h are Planck constant and Dirac constant respectively.

1.3 Vortex beams

The optical field is described via the maxwell's equations and the solution of optical field of the VB is solved by Helmholtz's equation under the condition of paraxial approximation. The light beam with a spiral wavefront possesses the property of OAM in each photon. Because of the uncertain azimuth angle in the center of VB, the position of optical axis of VB exists a phase singularity with the undefined phase and the modulus of zero. Hence, the intensity distribution of VB in the cross section is the bright ring with a hollow space in the center. The optical field of general VB along to the propagation direction of the z-axis can be represented by the following equation under the condition of the paraxial approximation

$$u(r,q,z)=u_0(r,z)exp(-ikz)exp(il\theta) \tag{1.33}$$

where the $u_0(r,z)$ denotes the complex amplitude and $exp\ (il\theta)$ is the item of the spiral phase along to the azimuth angle of θ. The unique spiral phase structure, promote many researchers to devote themselves to study on the method of generating the VB. In experiment, the common light beams with a spiral phase in the experiment have Laguerre-Gaussian and Bessel beam and so on.

1.3.1. Laguerre-Gaussian beam

Each photon of VB possessing the OAM that was first to be demonstrated by Allen in

1992 via the research on the Laguerre-Gaussian (LG) beam [30]. The LG beam is the most common light beam in experiment, possessing a spiral phase structure and many researches on the VB using the LG beam had a remarkable development. As the principle of wave equation, the intensity distribution of LG beam is derived from the Eigen solution of the Helmholtz equation under the condition of paraxial approximation, and the corresponding complex amplitude is expressed by

$$LG_{ml} = \sqrt{\frac{2m!}{\pi(m+|l|)!}} \frac{1}{w(z)} \left[\frac{\sqrt{2}r}{w(z)}\right]^{|l|} \exp\left[-\frac{r^2}{w^2(z)}\right] \{L_m^{|l|}\left[\frac{2r^2}{w^2(z)}\right]\} \exp(il\theta)$$

$$\exp\left[\frac{ikr^2 z}{2(z^2+z_R^2)}\right] \exp\left[-i(2m+|l|\tan^{-1}\left(\frac{z}{z_R}\right)\right] \tag{1.34}$$

where the m and the *l* indicate the radial index the topological charge respectively. *w(z)* and w_0 represent the size of the light spot at the propagation distance of z and the waist radius respectively. Moreover, the Z_R is the Rayleigh distance and $(2m+|l|+1)\tan^{-1}(z/Z_R)$ is Gouy phase. The generalized Laguerre polynomial is expressed by

$$L_m^{|l|} = (-1)^{|l|} \frac{d^{|l|}}{dx^{|l|}} L_{m+|l|}(x) \tag{1.35}$$

Figure.1.3 shows the phase and intensity distributions of the LG beam. The hollow dark space in the center is increased with the rise of the topological charge of *l* at a certain radial index of *m*. Similarly, the number of the bright rings is increased with the rise of radial index at a certain topological charge. Moreover, the radius of center bright ring is gradually decreased with the rise of the radial index. When the $m = 0, l \neq 0$, this type of LG beam is called as the TEM_{01} and the optical field is expressed by

$$E(r,\theta,z) = E_0 r \exp(il\theta) \exp\left[F_2(z) - \frac{\mathrm{r}^2}{F_1(z)}\right] \tag{1.36}$$

where the E_0 is the amplitude, and the $F_1(z)$ and $F_2(z)$ represent the spatial divergent and

phase shift function respectively.

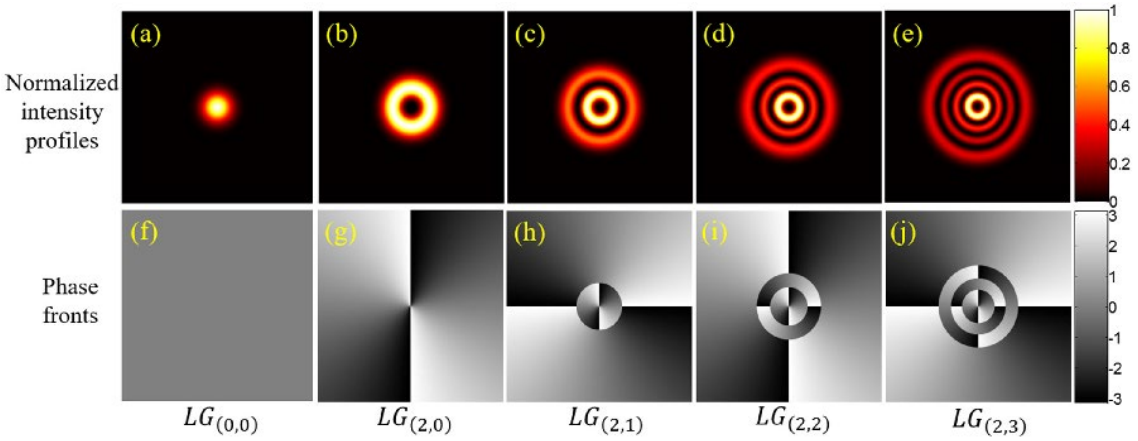

Fig.1.3 Intensity and phase distribution of LG mode with different order [31].

1.3.2 Bessel beams

The Bessel beam was first to be proposed by professor J. Durnin in 1987 [32]. The wave equation in free space had a particular solution, which can be described by the Bessel function. Hence, the corresponding light beam which is described by the Bessel function is called as Bessel beam. The optical field of the ideal Bessel beam is represented by

$$E(r,\theta,z) = E_0 \exp(ik_z z) J_l(k_r r) \exp(il\theta) \tag{1.37}$$

where the J_l is the l orders of the Bessel function of the first kind, and the k_z and k_r are the component of wave vector in the propagation and radial direction, respectively.

The intensity and phase distribution of the ideal Bessel beam are shown as in Fig.1.4 The zero-order of Bessel beam is the bright spot without the helix phase structure. The higher-order of Bessel beam, which is similar to the LG beam, yields a phase singularity in the center with a dark space. The intensity distribution of Bessel beam has the multiple concentric circles and the radius of the center ring is expressed by

$$r_l = \frac{\rho_l}{k_r} \tag{1.38}$$

The ρ_l indicates the position of the first maximal value starting from the center origin point for the l order of the Bessel beam. According to the Eq. (1.38), it found that the radius of the ring is only related to the Bessel function. Hence, the ideal Bessel beam remains unchanged characteristic under the process of propagation along to the propagation direction and it proves that the Bessel beam is a non-diffraction beam with infinite energy. Due to go against the conservation of energy, the Bessel beam can be not realized experimentally. Therefore, the general method for generating a Bessel beam is via the superposition of the Gaussian function to generate the Bessel-Gauss (BG) beam and the optical field is represented by

$$E(r,\theta,z) = E_0 \exp(ik_z z) J_l(k_r r) \exp(il\theta) \exp(-\frac{r^2}{w_z^2}) \tag{1.39}$$

In the specific condition, the BG beam can be considered as the non-diffraction light and even if it meets a tiny barrier, the complex amplitude can be recovered at a certain propagation distance. Due to this property, the Bessel beam has been widely used for optical communication.

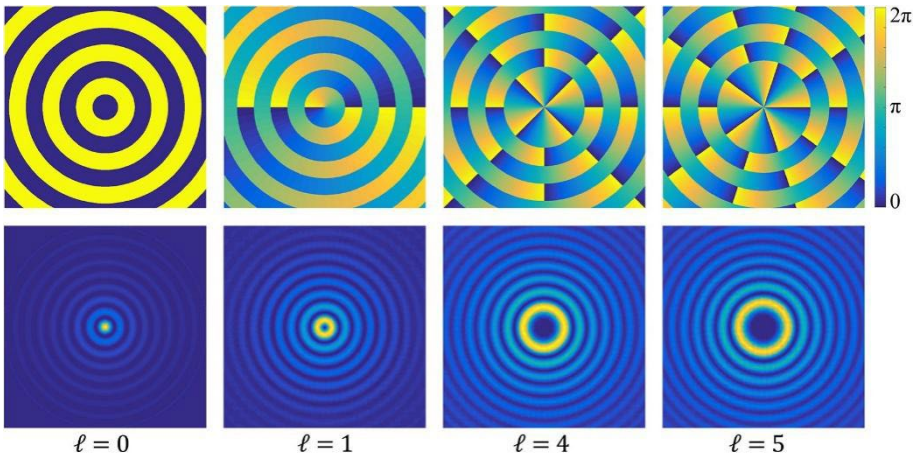

Fig.1.4 Intensity and phase distribution of Bessel mode with different order[33].

1.4. Method of generating the vortex beam

Due to the unique spiral phase structure, the researches on generating the VB have been attracted more attention to produce the high quality of VB. Many methods for the generation of the VB have been proposed and developed, which are mainly classified into two types for the laser mode modulation and the phase elements [34]. For example, the LG beam is the transverse mode of laser device. Hence, the laser mode modulation in the resonant cavity has been employed in generating the VB. Additionally, phase elements due to the more convenience has been widely utilized to generate the VB in experiment. Such as the spiral phase plate (SPP) and the spatial light modulator (SLM). Moreover, the hologram of the fork grating via the interference between the plane wave and VB was first to be employed on generation of the VB in 1992. Nowadays, the researches on the generation of the multi-wavelength VB and the higher order of VB have been developed. For example, the *q*-plate was proposed to generate the multi-wavelength VB and the reflection-type SPP was invented to produce the more than 10000 order of VB [35].

1.4.1 Spiral phase plate (SPP)

The spiral phase plate (SPP) is one types of the designed glass with a special helix staircase structure in the inside, that has been used for generating the VB via converting the surface of wavefront of Gaussian beam into the VB [36]. Figure.1.5 shows the process of the generation of VB by means of the SPP. The thickness of SPP in center is grown linearly with the rise of the azimuth angle and the thickness increment of Δd is given by $\Delta d=l\lambda\theta/[2\pi(n-1)]$ with the azimuth angle of θ and the topological charge of l, where the n and the λ are the refractive index of SPP and the wavelength of incident light, respectively.

Therefore, a Gaussian beam as the incident light into the SPP is added the phase increment of spiral phase of $\exp(il\theta)$ to the Gaussian beam after passing through the SPP. Consequently, the corresponding order of VB is generated by using the SPP. Figure.1.6 shows the 16 steps of SPP designed by the order of l=1 and the corresponding intensity distribution of the VB with the topological charge of l=1 was produced as shown in the Fig.1.6 (b). Similarly, the reflection-type SPP has been also used for generation of the higher order of VB and it realized that more than the 1000 orders of VB were generated successfully [37]. In recent years, the refection-type SPP used for the generation of the over 10000 orders of VB was successfully invented as shown in the Fig.1.7 [35].

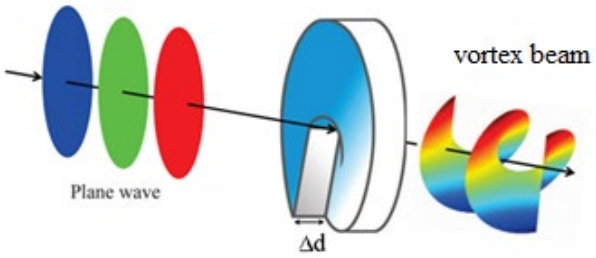

Fig.1.5 Schematic of generating optical vortex by spiral phase plate (SPP).

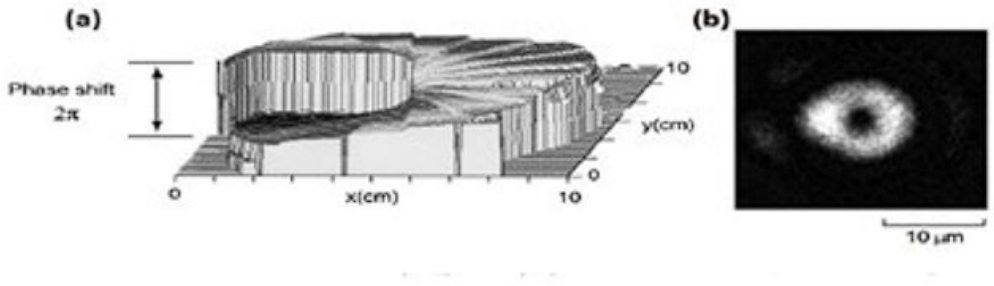

Fig.1.6 (a). Schematic of a step-type SPP, (b) pattern of the optical vortex with the topological charge of 1 generated by SPP [37].

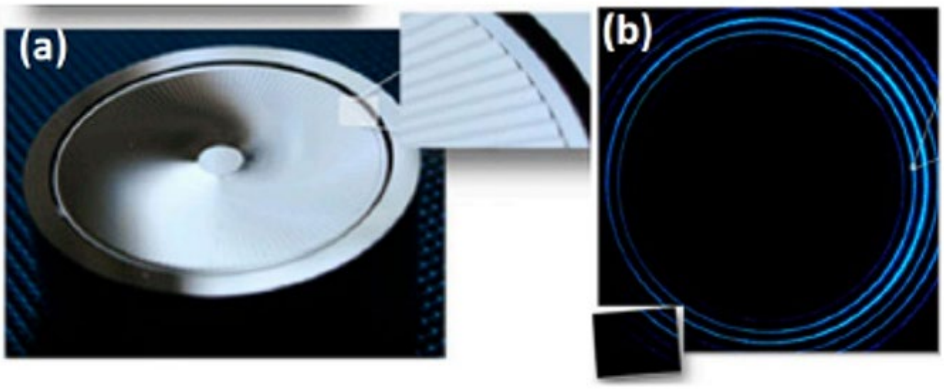

Fig.1.7 (a). Spiral phase mirror (SPM) for generating optical vortex with the topological charge of 10010, (b). pattern of generated optical vortex with the topological charge of 10010, which is stitched by 20 images by CCD[35].

1.4.2. Computer-generated holography

Based on the principle of holograph, the interference between the plane wave and the VB has been used for generating the fork grating hologram [38]. Due to the fork grating hologram containing the phase information of VB, the plane wave such as Gaussian been was used for matching the fork grating hologram. Consequently, a plane wave passing through a fork grating hologram led to generate a VB in the diffraction component. The interference between the Gaussian beam and the VB was applied for the generating the VB. The fork grating hologram is described by the intensity of interference fringe between the plane wave and vortex beam, as follows.

$$I = E_1^2 + E_2^2 + 2E_1E_2\cos(l\theta - kx\sin\phi) \tag{1.40}$$

Equation. (1.40) reveals that the hologram of fork grating is dependent on the item of $\cos(l\theta - kx\sin\phi)$. According this item, the fork grating hologram can be generated by numerical simulation. Figure.1.8 shows the fork grating with the order of l=1,3 generated by the interference between the plane wave and the corresponding the order of VB,

respectively. Moreover, figure.1.9 shows the process of generating the VB with the order of *l*=3. According to the general principle of the holograph, the generated diffraction light in the first and the negative first orders of diffraction component indicate the recovered VB with the order of *l*=+3, -3 respectively. With the development of hologram technique, the computer-generated hologram method has been widely utilized in experiment.

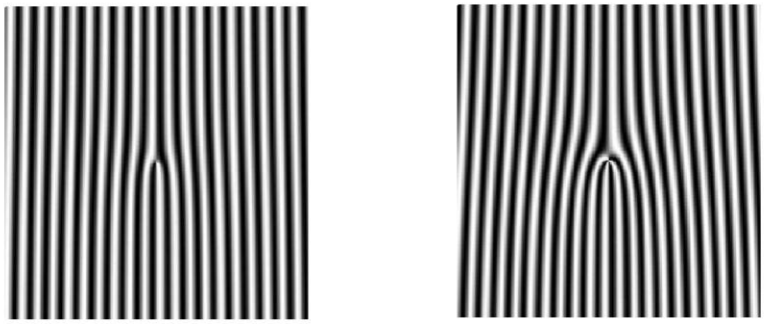

(a) (b)

Fig.1.8. The hologram of fork grating with the order of *l*=1,3 respectively.

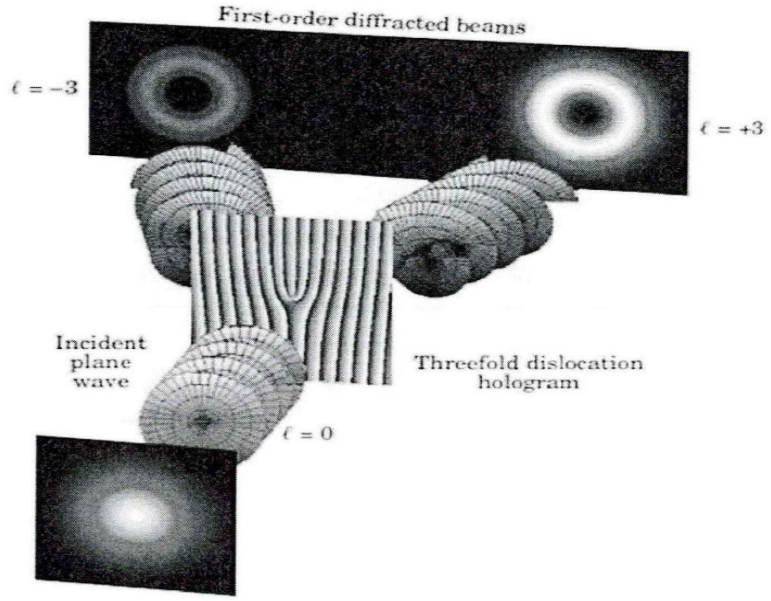

Fig.1.9. The diagram of generating the VB with the topological charge of *l*=3 via the hologram fork grating [39].

1.4.3. Spatial light modulator (SLM)

The SLM has the capacity of modifying the optical field spatially, which has been applied for the generation of VB [40]. The structure of SLM is combined with liquid crystal and the tropism of the liquid crystal can be controlled by computer. Moreover, each pixel in the screen of the SLM can be addressed with an 8-bit value, corresponding to a grey level on the display. Consequently, phase information of optical vortex in each pixel of SLM can be added to the incident light to modify the surface of wavefront of Gaussian beam and the obtained VB is generated by the reflected light beam from the SLM. Due to the flexible and programmable characteristic, it has been widely utilized to generate the VB in experiment. At present, the SLM can generate a maximum of 300 orders of VB [41]. Expect for the application of generating the VB, the SLM has been applied for the coding communication with the VB as well.

1.4.4 *q*-plate

Due to the property of spin angular momentum and orbital angular momentum of particle transforming each other, the *q*-plate has been applied to generate the VB. In 2006, Marruccui etc. found that a light beam passes through the inhomogeneous anisotropism crystals, leading to the spin angular momentum and orbital angular momentum of the photon transformed mutually [42]. According to this property, the *q*-plate has been employed to generate the VB. For the *q*-plate, the optical axis's direction of each liquid crystal molecule is changed spatially, and the optical axis's direction of α satisfies the equation of $\alpha=q\phi+\alpha_0$, where the q is the integer or half-integer and ϕ is the azimuth angle of *q*-plate. The a_0 indicates the constant. Figure.1.10 shows the process of generation of

the VB via a q-plate with the q of 1. The Gaussian beam with the left-hand circular polarization generated the right-hand circular polarization VB with the order of 2 after through the q-plate. On the contrary, the Gaussian beam with the right-hand circular polarization passes through the q-plate, and the left-hand polarization vortex beam with the order of -2 was produced. Hence the chirality of the VB is dependent on the chirality of the Gaussian beam from incident light with the circular polarization and the corresponding topological charge is related to the q value of q-plate.

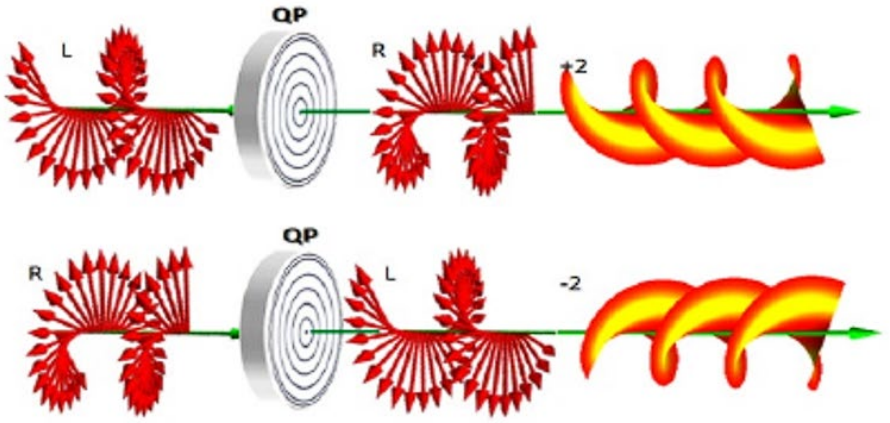

Fig.1.10. Schematic of generating optical by q-plate [43].

1.5. Applications of vortex beam

Due to the unique property of OAM, many applications with VB using this feature have been proposed. In the life science field, the feature of OAM generating the gradient force of electric field was utilized to capture the particle, making it rotate around the optical axis of VB. Due the high stability and the space division multiplex, the VB has been widely adopted in optical communication for the information store and coding

communication, and so on. Moreover, the VB can be as the depletion light to realize the super-resolution with high contrast. More and more researches on VB manifest that a huge development potential in quantum optics and optical detection.

1.5.1. Micromanipulation with the vortex beam

In the 1980s, Ashkin invented the optical tweezers [44] by means of the property of the gradient force of electric field generated by the laser to realize the capturing microscopic particle and controlling the directional movement of the particle. With the development of the application using the optical tweezers technique, it has gradually been become to be the one of most important instruments in the life science field. As the optical tweezers, Ashkin was awarded the Noble prize in physics in 2018. Inspired by this, in 1995, Rubinstein-Dunlop used the third-order of VB as the optical tweezers to successfully capture the absorbing particle [45]. Figure.1.11 recorded the absorbing particle at different moments, which shows that the particle was captured and rotated itself under the effect of the driving force from the VB. This study found that the focused VB can make particle rotate around the center of optical axis, which demonstrated that the property of OAM for the VB can be transferred to the particle. In 1997, Padgett controlled the relative chirality of two circular polarization of VBs to realize the controlling angular momentum of each photon in the range of 0 to $2\hbar$ [46]. Additionally, Garcés-Chávez demonstrated that the particle rotates around the center axis of the vortex beam in the condition that the size of VB is larger than the size of the particle [47]. Considering these studies of optical vortex tweezers, Lee summarized a theoretical basis for micromanipulation based on the state of particle motion affected by the property of the particle [48]. In 2002, Grier was first to propose the concept of holographic optical

tweezers, which utilized the VB for the coherent combining with the different types of the light beam to control the arrangement of multiple microscopic particles [49]. Moreover, Schmiegelow was successful to transfer the angular momentum of a VB photon into an electron [50]. Consequently, the manipulation with a VB can be applied for the smaller size of the particle. In recent years, the micromanipulation technique in the three-dimensional space with the VB had a significant development. Therefore, the application of VB in micromanipulation has a great potential.

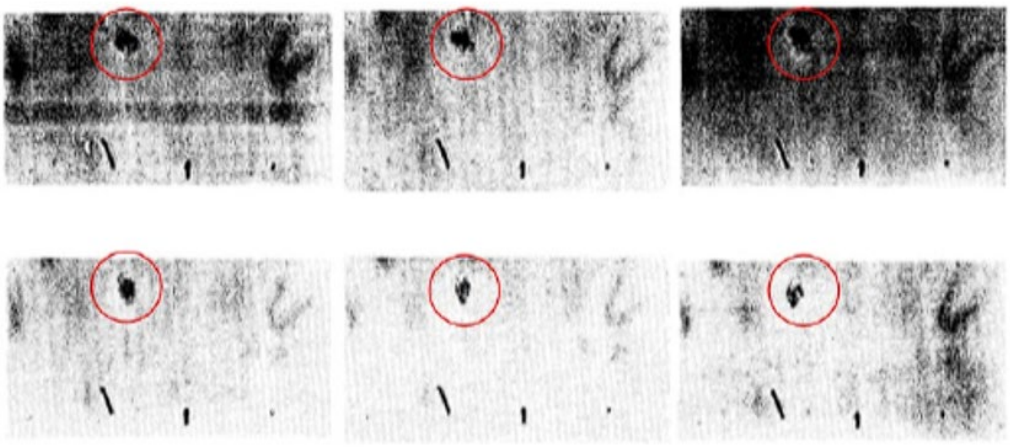

Fig.1.11. Six frames of the absorbing particle trapped by a vortex beam at different moments, the red circles denote the absorbing particle.[45]

1.5.2. Super-resolution imaging

The VB has a small size of the hollow dark space in the center under the condition of the low topological charge. Using this feature, the VB can realize the super-resolution imagine of microimaging. In 1994, Hell and Wichmann proposed a method of stimulated emission depletion (STED) for improving the resolution of microimaging [51]. The method utilized the Gaussian beam to stimulate fluorescence, meanwhile the longer wavelength of VB which is superposed in Gaussian beam has the effect of suppression of

fluorescence simultaneously. Therefore, the imaging with the fluorescence spot was only in the dark space and realized the improvement of the resolution of the image, going beyond the diffraction limit. Based on this property, several studies for using the VB to realize the super-high solution have been proposed and developed [52,53]. Similarly, researchers utilized Gaussian beam and the VB for scanning an object respectively. Consequently, the scanning images generated by means of Gaussian beam and VB respectively was subtracted mutually and an image with the high contrast was obtained [54].

1.5.3 Optical communication

With the development of optical communication in recent, the applications of VB in the optical communication field have been attracted a tremendous attention owing to the high stability and communication capacity. Based on the space division multiplex for various orders of VB, the capacity of optical communication can be enlarged [55,56]. In 2012, Willner, based on the polarization division multiplexing for the VB, realized the enlarging capacity of optical communication to the 2.56Tbit/s [55]. In 2015, Xiaocong Yuan used the Dammann grating for the space division multiplex for four VBs to expand the communication capacity to the 160Tbit/s [56]. Therefore, the VB has a large potential application background in expanding the capacity of optical communication. Additionally, the spatial phase information of VB can be used as the information coding. In 2004, Pledge utilized a spatial light modulator to modify the wavefront of the Gaussian beam to be divided into several different orders of VB and the corresponding with the topological charge were considered as the communication coding, realizing the light beam propagation distance in free space over 15 meters [57]. In 2014, Zeilinger etc.

realized the propagation distance of optical communication with the VB in free space reached to 3 kilometers, and the signal receiver and signal projector were across Vienna by means of the coding communication method [58]. Further, the light beam propagation distance in free space was improved to be more than 140 kilometers. Considering these applications, the VB has an enormous potential for optical communication and optical information storage.

1.6. Phase measurement methods for the vortex beam

The helix wavefront possessing the property of OAM which is related to the topological charge, is the one of most crucial parameters. Accurate measurements and estimations of the phase distributions and the topological charges are significant to guarantee the VB quality. Due to the phase distribution of VB being dependent on the topological charge, some methods based on the characteristic of interference and diffraction patterns of VB were first to be proposed for estimation of the topological charge of VB. For examples, the special diffraction aperture such as the triangle and circle aperture has been employed in estimating the topological via detecting the variation of diffraction patterns, which is associated with the topological charge. Nevertheless, these methods for the estimation of the topological charge were too rough due to the uncertain phase information. With the development of optical communication and the micromanipulation, the quantitative phase measurement method of vortex wavefront become to be significant and some wavefront sense methods based on the interferometric technique combining with the corresponding algorithms have been proposed and developed. Four-steps phase shift and heterodyne interferometry have been employed in phase measurement of VB due to the high measurement accuracy and sensitivity.

1.6.1 Four-step phase shift

The method of Four-step phase shift based on the basis principle of interference has been employed in the phase measurement. Due to the high measurement accuracy and the more convenient data processing, it is an excellent candidate for the phase measurement of the the VB. According to the interference principle, the interference phase is derived from 4 images with the phase shift of 0, π/2, π and 3π/2 respectively. The equation of phase is expressed by [59]

$$\varphi = \arctan \frac{I_4 - I_2}{I_1 - I_3} \tag{1.41}$$

where the I_1 ,I_2, I_3 and I_4 are the intensity of interference fringes with the phase shift of 0, π/2, π and 3π/2, respectively.

Figure.1.12 shows the schematic of the experimental setup for the phase measurement of VB via the method of four-step phase shift [22]. The VB was generated by a spiral phase plate (SPP) was interfered with a reference wave with the phase shift of 0, π/2, π and 3π/2, respectively. And the 4-stpes phase shift in reference wave were predefined by a SLM and the corresponding interference fringes with the phase shift were recorded by the CCD.

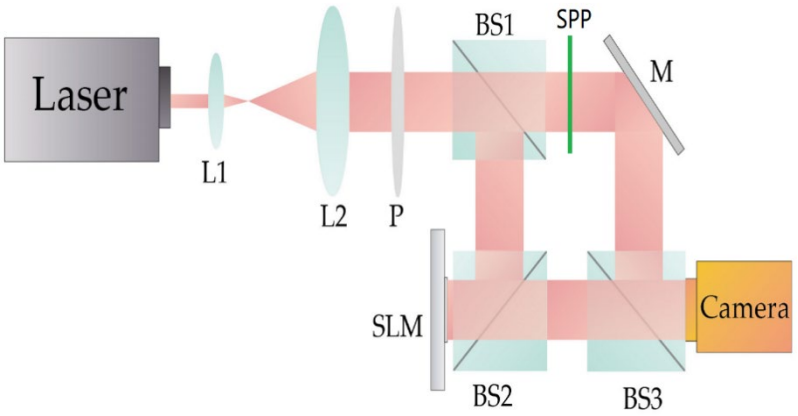

Fig.1.12. Schematic of the experimental setup. L_1 and L_2 are lenses with f=50mm and f=200mm, respectively. BS1, BS2, and BS3, beam splitters; SPP, spiral phase plate; M, mirror; SLM, spatial light modulator

Therefore, the predefined phase shift with the 0, π/2, π and 3π/2 were introduced to the reference wave, modulated by an SLM. To solve the interference phase containing with the VB, these interferograms between the reference wave and the VB with the phase shift of 0, π/2, π and 3π/2 were recorded respectively by a CCD image sensor. Therefore, the intensity of interferograms with the four-steps phase shift can be represented by [22]

$$I_{1n} = A_R^2 + A_0^2 + 2A_R A_0 \cos[(\varphi_R + (n-1)\frac{\pi}{2} - (\varphi_i + \varphi_v)] \tag{1.42}$$

Where the n is integer with the n= 1,2,3 and 4 respectively, and the A_R and A_0 are the amplitude of the reference wave and the object wave. The φ_R, φ_i and φ_v represent the phase of the reference wave, object wave and VB respectively. According to Eq. (1.41), the interference phase containing with VB can be directly obtained, given by $\varphi_1 = \varphi_R - (\varphi_i + \varphi_v)$. Similarly, the intensity of interferograms without the VB is given by

$$I_{2n} = A_R^2 + A_0^2 + 2A_R A_0 \cos[(\varphi_R + (n-1)\frac{\pi}{2} - \varphi_i] \tag{1.43}$$

and the corresponding interference phase without the vortex phase was obtained in the same manner, given by $\varphi_2 = \varphi_R - \varphi_i$. Hence, the phase of VB was deduced to be

$\varphi_v = \varphi_1 - \varphi_2$. Figure.1.13 shows the process of phase measurement of VB with the order of l=1.

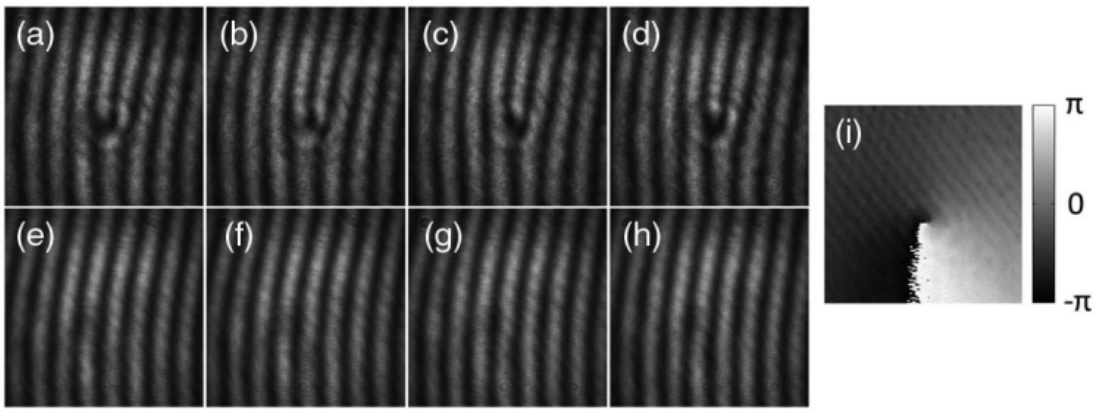

Fig 1.13. Hologram and phase images obtained by the phase-shifting digital interferogram. (a)–(d) Holograms formed by the interference between the vortex beam with a topological charge of 1 and the referenced beam with phase shifts of 0, π/2, π, and 3π/2, respectively. (e)-(h) Holograms formed by the interference between the incident beam without vortices and the referenced beam with phase shifts of 0, π/2, π, and 3π/2, respectively. (i) Phase image of the vortex beam with a topological charge of 1 [22].

1.6.2 Heterodyne interferometry

The heterodyne interferometry based on the discrete signal processing has been employed in the phase measurement [60] and an improved heterodyne interferometry was proposed for the phase measurement of VB, via data processing with least square method [23]. Figure.1.14 shows a schematic of phase measurement based on the heterodyne interferometry and the VB were generated by a vortex phase plate.

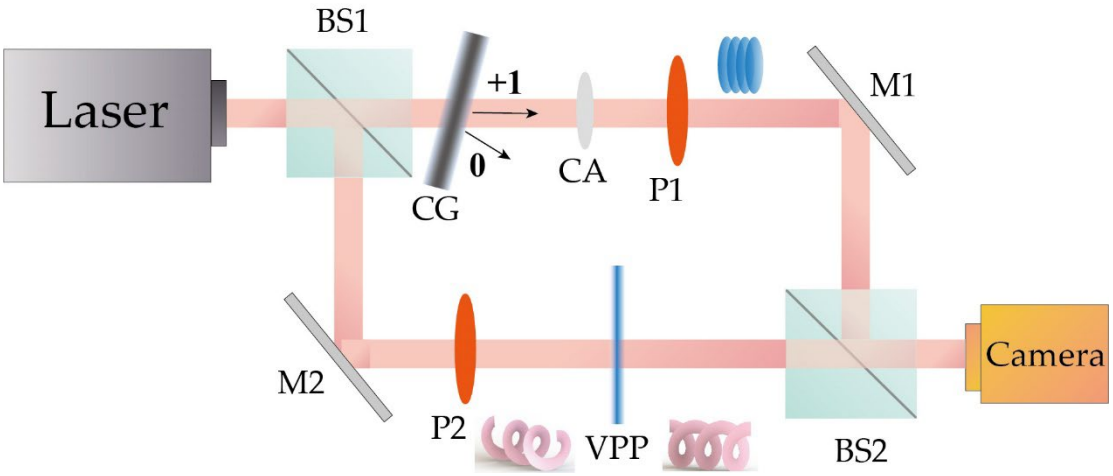

Fig.1.14 Experimental setup for phase measurement of the vortex beam based on heterodyne interferometry. Mirror, M1 and M2; non-polarization beams splitters, BS1 and BS2, polarizers, P1 and P2; VPP, vortex phase plate; circulating grating, CG; and circular aperture, CA.

A circulating grating (CG) in Fig.1.14 was rotated at a certain frequency, leading to the frequency shift in the reference wave signal. Consequently, a series of time-varying interference fringes were acquired by CCD. And the corresponding interference intensity in each pixel is expressed by [23]

$$\begin{aligned} I_i &= A_R^2 + A_0^2 + 2A_R A_0 \cos[\Delta\omega t + \Delta\varphi(x,y)] \\ \Delta\varphi(x,y) &= \varphi_v(x,y) + \varphi_p(x,y) - \varphi_r(x,y) \end{aligned} \tag{1.43}$$

where the A_R and A_0 are the amplitude of the reference wave and object wave, respectively. $\Delta\omega$ indicates the beat frequency between the reference and object wave. Moreover, $\varphi_v(x,y)$, $\varphi_p(x,y)$ and $\varphi_r(x,y)$ were the phase of VB, a light source in receiving plane, and reference light, respectively. The interference signal acquired by the discrete signal processing on times can be fitted to be cosine curve. Therefore, the interference phase of $\Delta\varphi(x,y)$ in each pixel can be obtained by calculating the cosine curve of interference signal via the least square method. Comparing with the interference patterns without the VB, the phase of VB can be obtained via the interference phase containing the VB subtracting the interference phase of plane wave (without the VB). Figure.1.15 shows

the measurement result of phase measurement of VB, comparing with the theoretical and measurement value.

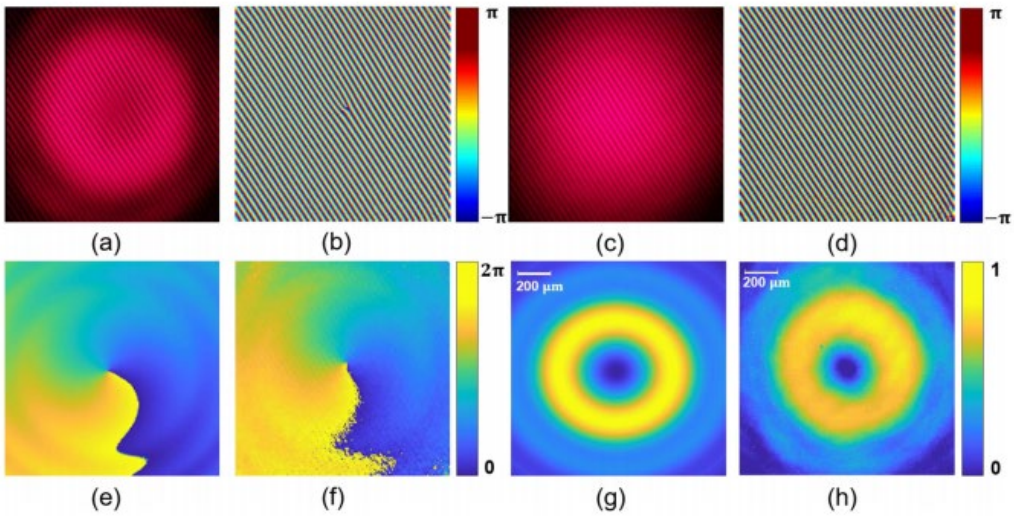

Fig. 1.15. Application of heterodyne interferometry on the measurement of the vortex with the topological charge of 1, at the propagation distance, z = 0.2 m. Interferograms of (a) the vortex beam interferes with the reference beam and (c) signal beam without vortices interfere with the reference beam; the calculated wrapped phase of (b) a vortex beam and (d) a non-vortex beam; theoretical results of (e) phase distribution and (g) intensity distribution; experimental results of (f) phase distribution and (h) intensity distribution [23].

1.7. Summary

In this section, we briefly introduced the concept of VB and the vortex wavefront was described. The unique helix wavefront is characterized by the spiral phase structure and yields a phase singularity with an undefined phase and the amplitude of zero. Therefore, the researches on generating the VB have been attracted attention and some methods using the phase elements such as the SLM, computer-hologram technique and *q*-plate have been employed in generation of VB due to the flexibility and convenient

configuration. Consequently, some light beam model with a spiral phase structure was proposed, such as the LG and Bessel beam. Give that these feature, the VB has a wide application in many fields. For example, the optical space division multiplexing for topological charge can be used for enlarge the capacity of optical communication. The optical tweezers using the focused VB to generate the gradient force of electric field, can capture the particle and make it rotate round the optical axis of VB.

Considering these applications with VB, the phase distribution of VB related to the topological charge for VB are one of the most crucial parameters. Therefore, the quantitative measurements and estimations of phase distribution and topological charge are significant to guarantee the VB quality and improve the efficiency of application. The estimation method of topological charge via detecting the interference and diffraction patterns was first to be proposed for estimating the topological charge. principles were proposed. Nevertheless, it is far from enough due to the uncertain phase information. For the requirement of quantitative estimation of the topological charge in some fields, the phase sensitive interferometry with phase shift algorithm and the improve heterodyne interferometry using the least square method have been employed in phase measurement of VB.

2. Sinusoidal phase modulation interferometry

The phase sensitive interferometry has been employed in phase measurement of the VB due to the high measurement and sensitive, such as the phase shift with four-step phase shift algorithm and the improved heterodyne interferometry using the least square method for data processing. Nevertheless, these methods have some obvious disadvantages. In the four-step phase shift algorithm, the least three predefined phase shift and thus corresponding interferograms were required. However, a slight deviation in phase shift may lead to an enormous noise in measurement result. As the heterodyne interferometry, the interference signal was generated by the discrete signal processing from the acquisition of variation of 2-D interference patterns in times. However, the obtained interference signal is commonly under the low frequency which is susceptible to be disturbed by the noise. Moreover, it may lead to no ideal result in the fitting result. Comparing with these methods, a SPM method has some obvious advantages in the higher controllable sampling frequency and the more straightforward calibration.

In this chapter, the schematic of an SPM interferometry for phase measurement of VB is introduced which is established by a modified Michelson interferometer [24]. The sinusoidal vibration in mirror to generate the sinusoidal modulation signal was added to interference signal and the corresponding equation of intensity of interference signal was given. Moreover, the analysis of noise in interference signal reveals that the suitable modulation amplitude of sinusoidal signal was given by z=2.63.

2.2. Schematic of the SPM interferometry

The SPM interferometry which is modified by a Michelson interferometer via a mirror attached piezoelectric transducer (PZT) has been adopted in the phase measurement [61,62], and a scheme of the SPM interferometry using a SLM to generate the VBs was proposed for achieving the phase measurement of VB due to the high measurement accuracy and more convenient configuration [24], as shown in Fig.2.1.

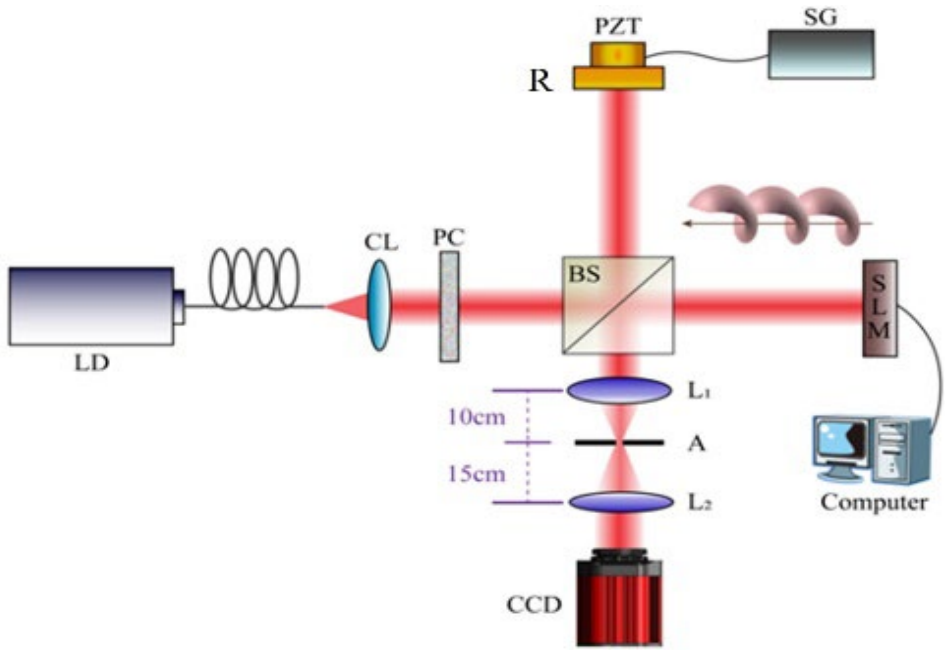

Fig. 2.1. Experimental setup of the interferometer with SPM configuration for measuring phase distributions of the optical vortices. LD, CL, L1 and PC represent a laser diode with a wavelength of 780 nm, collimator lens, and polarization controller, respectively. The reflect mirror was attached to a PZT for conducting phase modulation, where R is the reference mirror. The L1 and L2 are lenses with the focal lens of f1=10 cm and f2=20 cm respectively, Gaussian beam from LD was converted to VB via SLM.

In experiment setup, a laser diode with a center wavelength of 780nm as an incident light was divided into two beams by a non-polarization beam splitter (BS). One beam as a reference wave signal was reflected from a mirror which was the sinusoidally vibrated

by a PZT with a signal generator. Consequently, the sinusoidal modulation signal was added to the reference wave signal. Another beam as an object wave signal was reflected from an SLM which displayed the predesigned the hologram of phase mapping of VB on the screen to convert the surface of the Gaussian beam into VB. These two beams were recombined by the BS and interfered each other. Therefore, the continuous variation of 2-D interference patterns in times was recorded continuously by a CCD image sensor at a certain frame rate of f_{FPS}=1000Hz. A sinusoidal signal with a modulation frequency f_m was considered as sinusoidal modulation in the reference wave signal. The modulation frequency f_m of the sinusoidal signal and frame rate of the CCD, f_{FPS}, are synchronized and in a multiplicative relationship. In this experiment, we set the modulation frequency to f_m=125Hz, which is equivalent to one eighth frame rate of f_{FPS}. For obtaining sufficient discrete points to structure the interference signal, a period of interference signal contains 8 frames of interference patterns, and the 64 frames of interference patterns were sampling over 8 periods.

2.3. Principle of sinusoidal phase modulation method

2.3.1. Interference signal with a sinusoidal modulation

According to the discrete signal processing in practical, the continuous time-varying interference signal with a sinusoidal modulation in each pixel of interference fringe was constructed by a series of periodic discrete points. Hence, the time-varying interference signal of *s(x,y,t)* in each pixel of interference fringe can be represented as follows [61].

$$s(x, y, t) = s_0(x, y)\cos[z\cos(\omega_c t + \phi) + \alpha(x, y)] \tag{2.1}$$

where the s_0 (x,y) indicates the amplitude of interreference signal and the ϕ and ω_c are the initial phase and the angular frequency, respectively. Furthermore, the item of *a(x,y)* represents the phase difference in the pixel of interference fringe between the surface of the SLM and the Mirror where the x and the y are spatial coordinate of lateral and vertical axes, respectively. The z is modulation amplitude in terms of the radian phase value which is given by the $z = (4\pi/\lambda)\, a$, where the a is the amplitude of sinusoidal signal. Considering the effect of noise in measurement result, the noise mainly was classified by the multiplicative and additive noise, given by the $n_M(t)$ and $n_A(t)$ respectively. The multiplicative noise means the fluctuations of phase a in times caused by vibration of the optical devices. According to the analysis of interference signal independently, the effect of multiplicative noise in measurement result can be ignored. The additive noise occurs mainly in electronic devices. The modulation amplitude of z is dependent on the relation of the multiplicative and additive noise, which is described in next section.

.

2.3.2. Equation of phase distribution

To solve the phase $a(x,y)$, we perform the Fast Fourier Transform (FFT) for interference signal in each pixel of interference pattern. Hence, we obtain the m-order component of interference signal in frequency domain as follows [61]:

$$\begin{aligned} F(2m\omega_c) &= (-1)^m \mathrm{s}_0 \cos(\alpha) J_{|2m|}(z) \exp(j2m\phi) \\ F[(2m-1)\omega_c] &= (-1)^m \mathrm{s}_0 \sin(\alpha) J_{|2m-1|}(z) \exp[j(2m-1)\phi] \end{aligned} \tag{2.2}$$

where the $J_m(z)$ is the m-order Bessel function of the first kind and the m is integer. Under the condition of $-1/4\pi < \phi < 1/4\pi$, the phase difference as vortex phase can be represented by using the relation of $F(\omega_c)$ and $F(2\omega_c)$, given by [61]

$$\tan(\alpha) = \frac{\{|F(\omega_c)|/|J_1(z)|\}\,\mathrm{sgn}\{-\mathrm{Re}[F(\omega_c)]J_1(z)\cos\theta\}}{\{|F(2\omega_c)|/|J_2(z)|\}\,\mathrm{sgn}\{-\mathrm{Re}[F(2\omega_c)]J_2(z)\cos 2\theta\}} \tag{2.3}$$

Equation. (1.46) indicates the value of z is required and must be determined in advance. The value of z is associated with the noise. First, the value of z can be determined from the relation between the measured values of $F(3\omega_c)/F(\omega_c)$ and $R_{31} = J_3(z)/J_1(z)$. According to the theoretical analysis for effect of noise in practical measurement, the practical value of z should have a limit region of approximately 2.5-2.7 rad. By the analysis of interference signal from the effect of additive noise with the multiplicative noise in signal to noise ratio (SNR), the theoretical analysis of SNR of interference signal of s(x,y,t) based on effect of the additive noise and the multiplicative noise independently reveals that z=2.63 rad [61] is the most suitable amplitude for practical measurements. Owing to the monotonically decreasing curve of R_{31} as a function of z, the amplitude value of z can be uniquely and accurately determined in this range.

2.4. Summary

In this section, the schematic of an SPM interferometry was introduced. A SLM was used for generating the VB, and sinusoidal modulation signal was introduced into the reference wave signal via a mirror attached to PZT with a signal generator. The interreference signal was constructed via the discrete signal processing from the continuous variation of pixel of interference pattern in times. Equation of phase distribution of VB can be directly obtained by the FFT with the relation of $F(\omega_c)$ and $F(2\omega_c)$,. According to the analysis of interference signal from the effect of noise in measurement, the suitable modulation of z was given by 2.63 and the effect of noise in measurement result can be ignored.

3. Experimental results

We successfully generated the VBs with the integer and fractional order of VB via the spatial light modulator (SLM). The wrapped phase distribution of VB was directly obtained by means of FFT with the relation of $F(\omega_c)$ and $F(2\omega_c)$. For estimation of topological charge of VB, phase unwrapping method based on polar coordinates was proposed to determine the maximum continuous variation of phase in the phase measurement of VB. Moreover, to eliminate and reduce the effect of phase singularity and background in phase distribution of VB, the method of eliminating the part of phase singularity based on the measured intensity distribution of VB was proposed. Finally, the measurement result of topological charge was evaluated by the average value and the standard deviation was used for evaluating the stability of the repeated measurement. Moreover, the fluctuation of wavefront of Gaussian beam reveals the potential measurement error in the free space propagation,

3.1. Generation of the vortex beam

Many methods of generating VB have been proposed and developed. In experiment, a SLM was adopted to generate the VB, and the SLM allows flexible control of the transverse mode. The linear polarization of light beam with amplitude and phase can be modified spatially via the uploaded hologram of phase mapping on SLM. Hence, the predesigned hologram of phase mapping of VB with the order of l=1, 2, 3, 4, and 5 respectively was designed by computer and uploaded into SLM to display on the screen of SLM, as shown in Fig.3.1.

Fig.3.1 The hologram of phase mapping of vortex beam with the order of l=1,2,3,4 and 5 respectively.

Nevertheless, the obtained intensity distribution of VB is the multiple concentric circles around the center due to the diffraction on the surface of SLM, where the first maximum value of intensity of bright ring of VB is considered as the obtained VB. To eliminate the effect of diffraction rings, the pinhole was untiled to block the diffraction ring and only the VB can be pass through the pinhole. These two lenses in experimental setup were used for collimating the light beam. Consequently, the obtained VBs were acquired by a CCD image sensor. The intensity distribution of VB with the order of l=1,2,3,4 and 5 respectively were successfully obtained as shown in Fig 3.2.

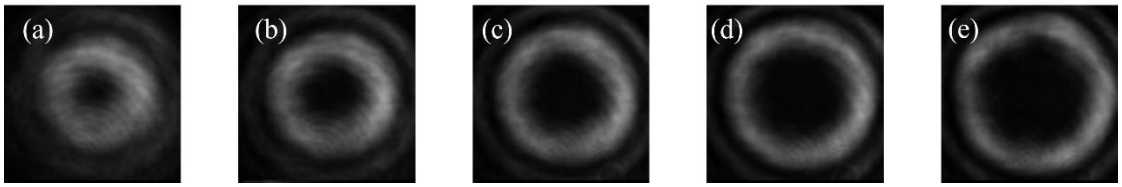

Fig.3.2 The intensity distribution of vortex beam with the order of *l*=1,2,3,4 and 5 respectively.

3.2. Interference patterns with sinusoidal modulation.

To obtain the continuous time-varying sinusoidal modulation interference signal, the period sinusoidal modulation generated by a sinusoidal signal was added to reference wave signal and the continuous variation of 2-D interference fringes in times were

acquired by a CCD at a certain sampling frequency. One frame of interference patterns with the order of *l*=1,2,3,4 and 5 respectively, were shown in Fig.3.3

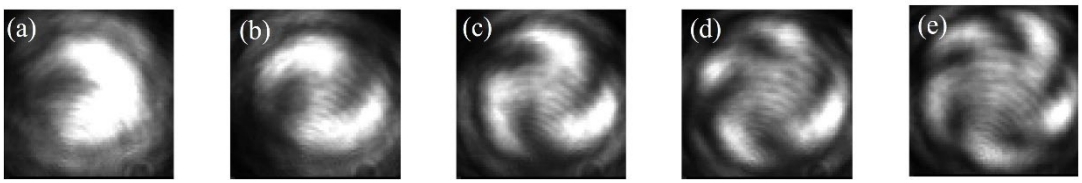

Fig.3.3 The intensity distribution of interference patterns between the Gaussian and vortex beam with the order of *l*=1,2,3,4 and 5 respectively.

As aforementioned scheme, the obtained interference signal from each pixel of interference pattern includes with 8 periods of interference patterns and a periodic interference signal was constructed by 8 discrete points from 8 frames of interference pattern. Figure.3.4 shows the obtained interference signal from the Fig.3.3 (c) at the position of x=23 and y=22 pixel, which was constructed by 64 frames of interference over 8 periods. For obtaining the whole phase information, the interference signal in each pixel of interference pattern were obtained in same manner, which were similar to the Fig.3.4. The modulation amplitude of z for the obtained interference signal were modulated to be approximately z=2.63.

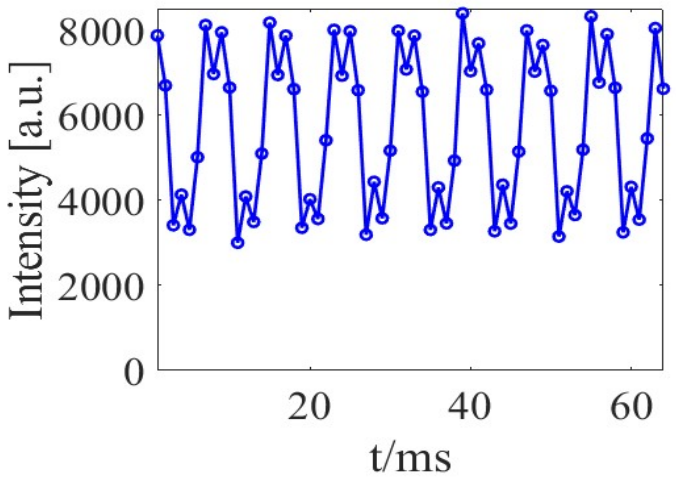

Fig.3.4 The interference signal with 8 periods in pixel of (23,22) of Fig 3.4 (a).

To solve the phase, we performed the FFT for interference signal and each frequency component of interference signal can be obtained which is described as Eq. (1.45). According to Eq.(1.46), the phase distribution of VB can be directly obtained via using the relation of $F(\omega_c)$ and $F(2\omega_c)$. The wrapped phase distribution of VB with the order of l=1,2,3,4 and 5 respectively were shown in Fig.3.5.

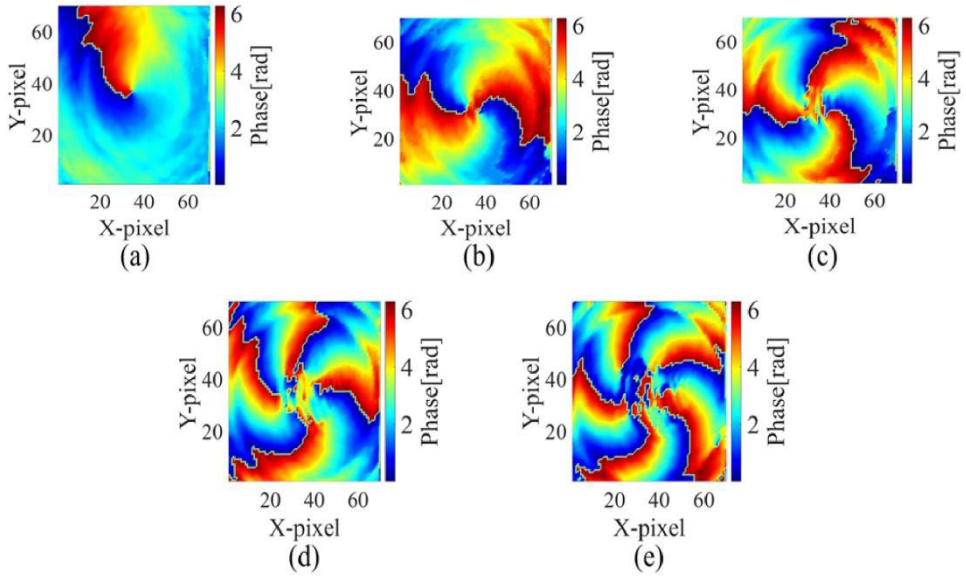

Fig. 3.5. The wrapped phase distribution of the VB with topological charge of (a) l=1, (b) l=2, (c) l=3, (d) l=4, and (e) l=5, respectively.

Figure.3.5 reveals that the variation of the azimuth angle along to the clockwise direction were approximately 2π, 4π, 6π, 8π and 10π respectively, which are corresponding to the topological charge of *l=1,2,3,4* and *5,* respectively. Hence, the topological charge of VB is defined by the equation of $l=\varphi_{max}/2\pi$, where the φ_{max} indicates the continuous maximum variation of phase in phase distribution of VB along to azimuth angle. For more precious to estimate the topological charge quantitatively, accurate measurement of maximum variation of phase is required to estimate the topological charge quantitatively with the high measurement accuracy. Therefore, the phase unwrapping method is necessary. In conventional method of phase unwrapping, the phase unwrapping algorithm based on the Cartesian coordinates was conducted along to the x-axis and y-axis respectively. It is difficult to distinguish the phase singularity and even the discontinuous phase distribution may be occurred in the phase unwrapping processing. To avoid this issue, the phase unwrapping algorithm based on the polar coordinates was adopted for the phase unwrapping of VB in this thesis. This method can clearly distinguish the position of phase singularity and the result of unwrapped phase has high measurement accuracy owing to the property of continuous phase. Figure.3.6 shows the process of phase unwrapping for the second order of VB. In Fig.3.6(a), the obtained wrapped phase distribution of VB with the order of l=2 was obtained under the Cartesian coordinates with the x-axis and y-axis. For Fig.3.6(a), the wrapped phase distribution can be represented under the polar coordinates along to azimuth angle in clockwise direction with the radius and azimuth angle as shown in fig.3.6(b), where the horizontal axis represents the sequence of points along the azimuthal angle at the same radius. Then, the unwrapped phase distribution of VB under the polar coordinates was obtained as shown in Fig.3.6(c). Finally, Figure.3.6 (d) was the unwrapped phase distribution under the Castain coordinates via

retransforming coordinates for Fig.3.6 (c).

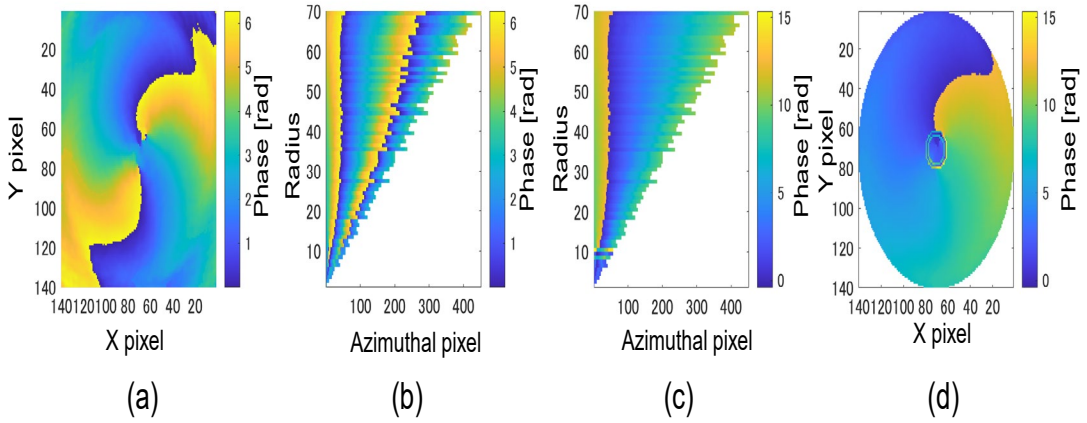

Fig. 3.6. Process of phase unwrapping specialized for optical vortices, (a) obtained phase distribution by SPM, (b) Coordinate transformed phase distribution. The horizontal axis represents the sequence of points along the azimuthal direction of the same radius. (c) unwrapped phase distribution with new coordinate, and (d) Re-transformed phase distribution.

In the Fig.3.6 (d), the maximum variation of phase of VB can be determined along to azimuth angle in clockwise direction between the origin of azimuth angle and the end of azimuth angle under the condition of the same radius. Due to the property of spiral phase structure, the phase step was shown in the vertical line direction between the origin point of azimuth angle and end point of azimuth angle at the same radius, which is considered as the maximum variation of phase at the same radius. In the Fig.3.7, the value of phase step was determined to be approximately 4π, which is marked by a red arrow.

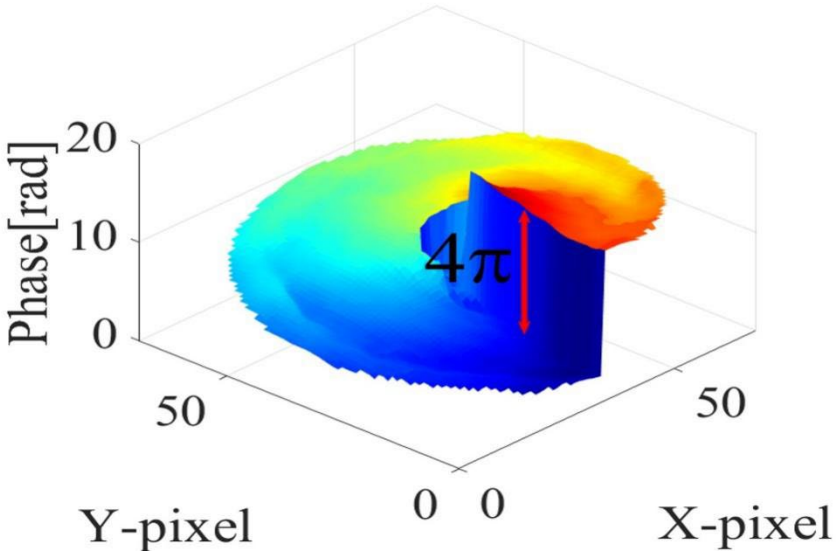

Fig. 3.7. The obtained unwrapped phase distribution of vortex beam with the order of *l*=2. The phase step is marked by a red arrow, which is approximately 4π.

Due to the phase singularity with an undefined phase existed in the center of VB, it has effect on the estimation of topological charge. We proposed a method via the measured intensity of VB to reduce the effect of phase singularity and background light based on the obvious intensity difference of the VB between the bright ring and the part of phase singularity. The measured intensity of VB with the order of l=1,2,3,4 and 5 were obtained by the measured unwrapped phase distribution of VB, represented by the absolute of complex amplitude, as shown in Fig.3.8. Because that the measured pixels of intensity in Fig.3.8 are consistent with the pixels in the measured unwrapped phase distribution of VB, a threshold value of 50% of the measured intensity distributions in Fig.3.8 was set and only the corresponding the position of intensity pixels in unwrapped phase of VB was highlighted without the background light and the part of phase singularity by removing the area which is below this threshold from the two-dimensional unwrapped phase

distribution, as shown in Fig.3.9 with the topological charge of l=1,2,3,4 and 5 respectively.

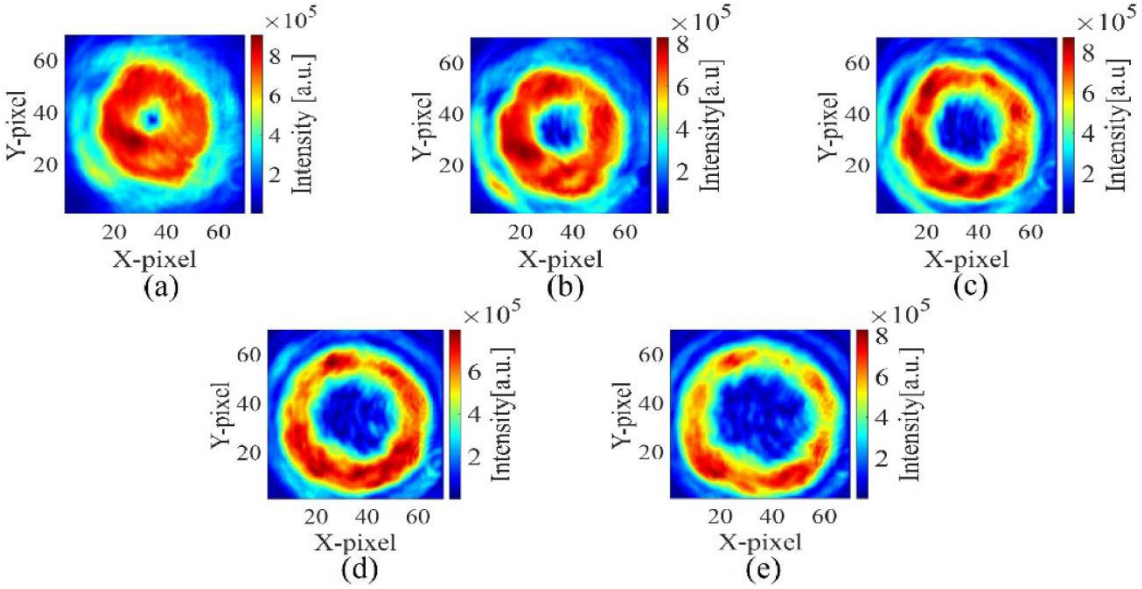

Fig. 3.8. The measured intensity distributions of the VB with topological charge of (a) *l*=1, (b) *l*=2, (c) *l*=3, (d) *l*=4, and (e) *l*=5, respectively.

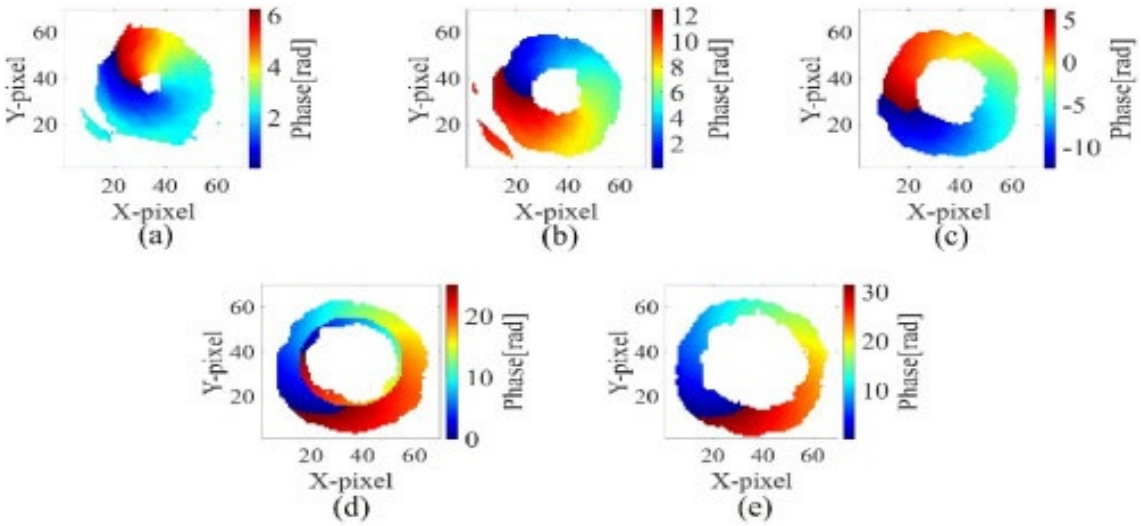

Fig.3.9. The unwrapped phase distribution of the VB showing only the light intensity components above 50% of maximum value of topological charge of (a) l=1, (b) l=2, (c) l=3, (d) l=4, and (e) l=5.

The effect of the phase singularity and background or diffraction light in unwrapped phase distribution of VB were effectively reduced. In the Fig.3.10 (a), the unwrapped phase distribution of VB with topological charge of l=1 was obtained which was represented by the polar coordinates along to the azimuth angle in clockwise direction at the same radius, as shown in Fig.3.10 (b). The phase differences between the phase value of the origin and end point along to azimuth angle in clockwise direction were obtained as shown in Tables.1 and 2, in the radius with the range of 25 to 35 pixels. Therefore, the values of phase step which is marked by a red arrow were determined by the phase difference and the measurement results of topological charge can be obtained as show in Fig.3.11 over 11 measurements.

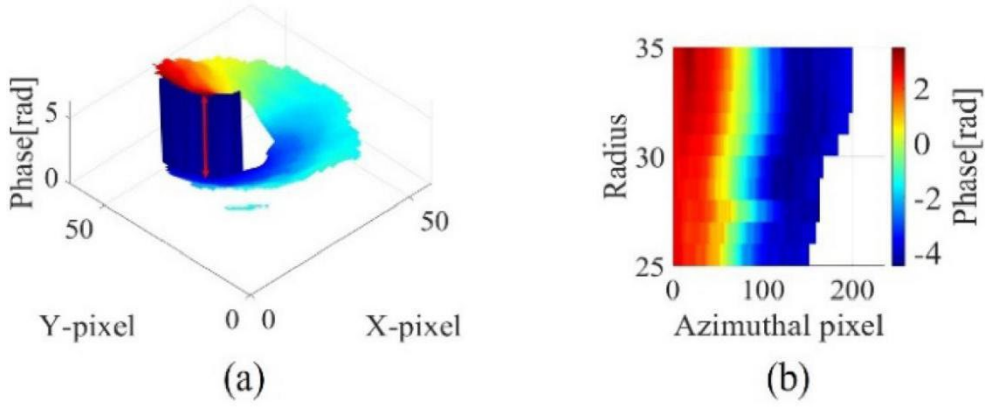

Fig. 3.10. Example of topological charge estimation for first order VB. (a) Extracted phase distribution of the VB with a first-order topological charge. (b) Phase distribution of Fig.8 (a) was represented by the polar coordinates along to the clockwise direction within the radius of 25 to 35 pixels.

Table 1. Phase difference (PD) between the phase value in the azimuth angle (0) [rad] and the azimuth angle (2π) [rad] on the clockwise direction

Radius [pixels]	25	26	27	28	29	30	31	32
Phase of azimuth angle (0) [rad]	2.561	2.440	2.459	2.523	2.591	2.592	2.605	2.593
Phase of azimuth angle (2π) [rad]	-3.905	-3.876	-3.846	-3.753	-3.753	-3.678	-3.679	-3.732
PD [rad]	6.466	6.316	6.305	6.276	6.344	6.270	6.284	6.325

Table 2. Phase difference (PD) between the phase value in the azimuth angle (0) [rad] and the azimuth angle (2π) [rad] on the clockwise direction

Radius [pixels]	33	34	35
Phase [rad] of the azimuth angle of 0 [rad]	2.594	2.622	2.604
Phase of the azimuth angle of 2π [rad]	-3.674	-3.606	-3.693
PD [rad]	6.271	6.228	6.297

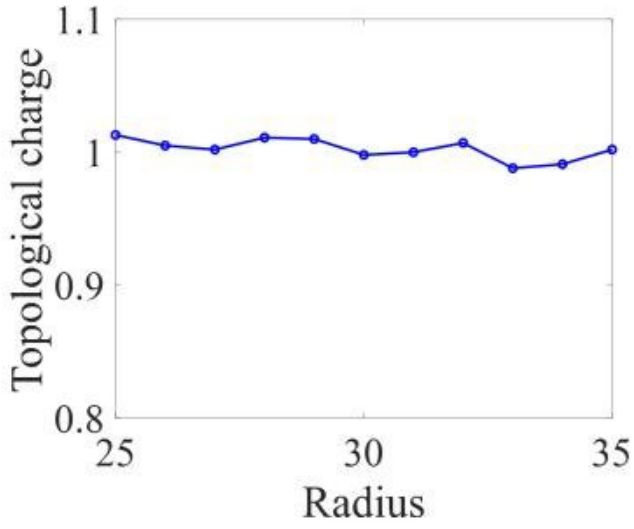

Fig.3.11. The topological charge of a VB with *l*=1.

To determine the topological charge, the VB with the topological charge of *l*=2,3,4 and 5 were determined in the same manner. The value of phase step without the phase singularity was successful to be obtained and the 11 measurements results of topological charge were shown in Fig.3.12 with the topological charge of *l*=2,3,4 and 5 respectively. The measurement accuracy was evaluated by the measured average of topological charge over 11 measurements. Comparing to the set value of topological charge as theoretical value in SLM, the measurement error was estimated within 4% and the corresponding standard deviation (STD) of 11 measurements was determined to be approximately in range of 0.010 to 0.016 rad, as shown in Table.3. which reveals the consecutive measurements of topological charge were stable over 11 measurements.

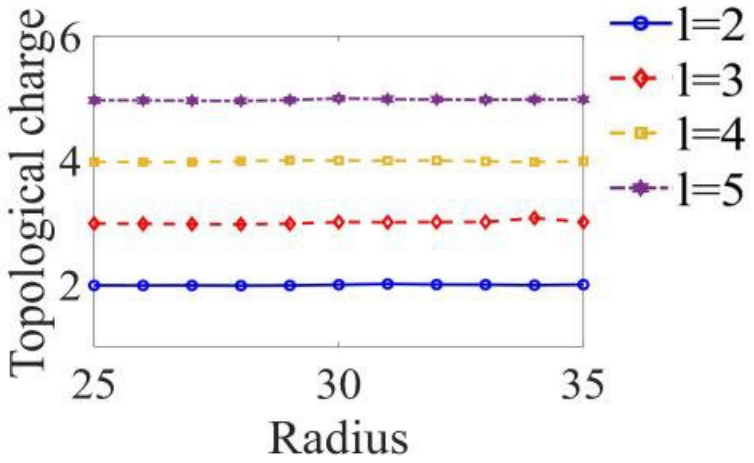

Fig.3.12. The topological charge of a VB with *l*=2, 3, 4 and 5 via 11 measurements, respectively.

Table 3. The Measured Errors of the topological charges

Theoretical value	1.000	2.000	3.000	4.000	5.000
Average value	1.002	1.992	2.998	3.984	4.983
Error [%]	2	4	0.6	4.0	3.4
STD [rad]	0.013	0.010	0.020	0.015	0.016

3.3. Measurement of the fractional order of vortex beam

The SPM method is an wavefronts measurement technique based on interferometric principle, has been employed in phase measurement of wavefronts. Recently, some methods of the phase measurement of the fractional order of VB have been proposed [55]. However, because of phase singularity and the defect of phase in phase distribution of VB, the experimental setup for the measurement of the fractional order of VB is too complex. In this thesis, the SPM method was adopted to be used for measuring the fractional order of VB in more convenient configuration. Because the phase measurement with high measurement accuracy can be obtained if a crisp interference pattern is obtained. The fractional order of VB can be obtained by a SLM. Nevertheless, due to the

background light in the position of defect of phase distribution and strong effect of diffraction for intensity distribution of the fractional order of VB occurred by SLM, it is difficult to directly obtain the crisp intensity distribution of the fractional order of VB. To eliminate the effect of diffraction and background light, the hologram of phase mapping of VB was generated by the SLM and meanwhile the hologram of blazed grating was used for combing with the hologram of phase mapping of VB to design the fork grating. Figure.3.13 was shown the designed the fork grating with the topological of l=2.5. The corresponding intensity distribution of the fractional orders of VB were produced in the first order of diffraction component, as shown in Fig.3.14. The wrapped phase distributions with the order of l=2.5, 3.5 and 4.5 respectively were obtained by the same method, as shown in Fig.3.15.

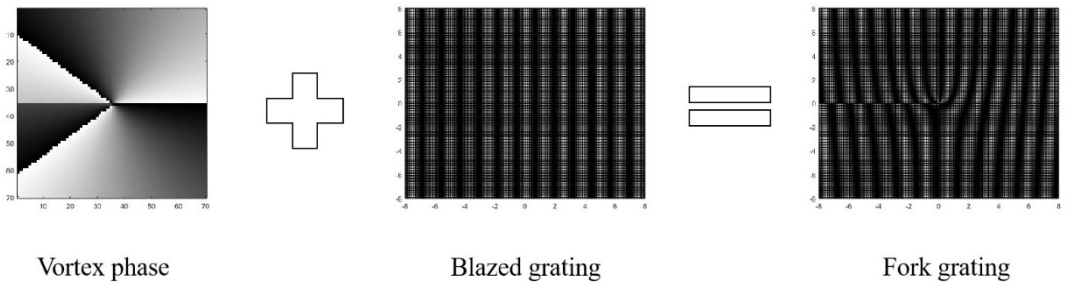

Fig.3.13. The process of generating the hologram of fork gratin with the topological charge of *l*=2.5.

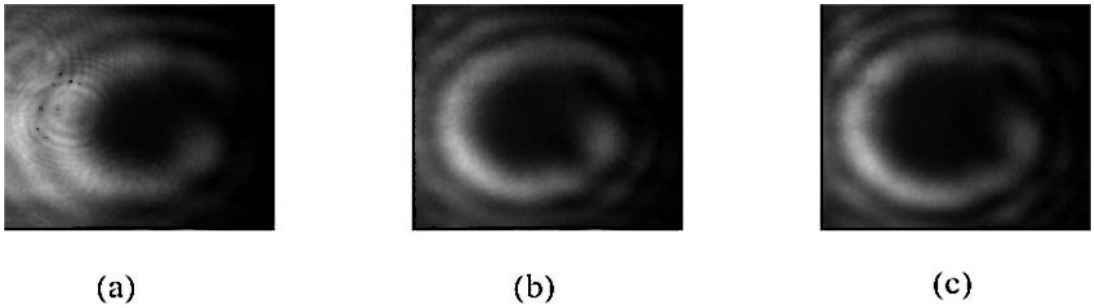

Fig.3.14. Obtained intensity distribution of vortex beam with fractional order of (a) l=2.5, (b) l=3.5, and (c) l=4.5.

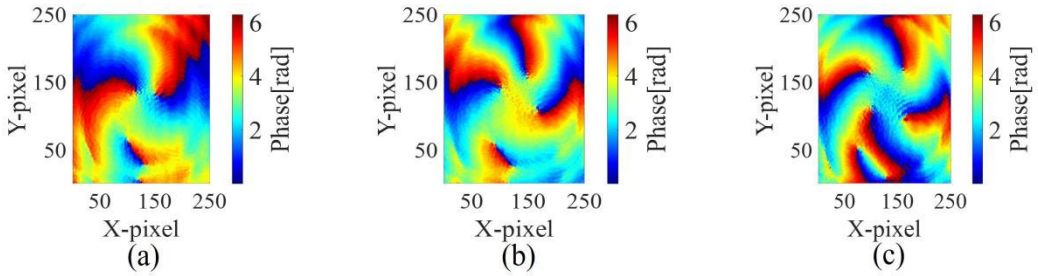

Fig.3.15. Obtained phase distributions of vortex beam with fractional order of (a) l=2.5, (b) l=3.5, and (c) l=4.5.

As the aforementioned method, we conducted unwrapped phase algorithm for the phase distributions of Fig.3.15. In the unwrapping process, the background or diffraction light from the SLM was eliminated and reduced effectively. Figure.3.16 shows the results of phase unwrapping without the part of phase singularity and indicates that crisp phase distribution of the fractional order of VB containing defect in the phase distribution.

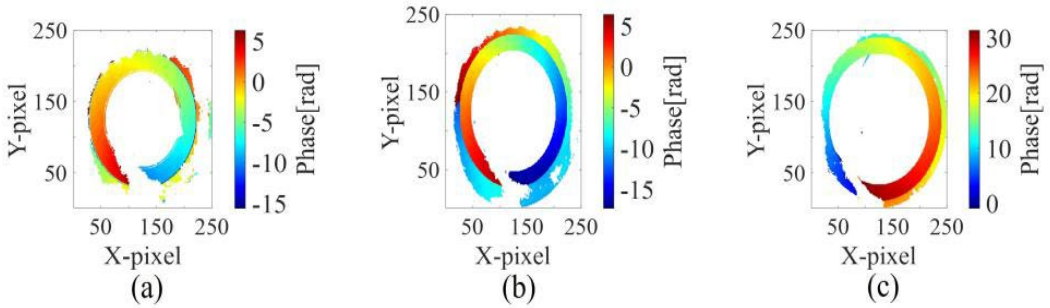

Fig.3.16. The unwrapped phase distribution of the VBs with the topological charge of (a) $l = 2.5$, (b) $l = 3.5$ and (c) $l = 4.5$, respectively.

In theory, the maximum phase variation of the VB can be determined in the phase distribution of VB along to the azimuth angle in clockwise direction between the origin point and the end of azimuth angle at the same radius. For Fig.3.16, the repeated measurements of maximum phase variation were determined along to azimuth angle at different radius, and the average of phase variation for the repeated measurements were estimated to be approximately 16.005, 25.425 and 27.961 rad. The corresponding average value topological charges were determined to be approximately 2.5487, 3.6322 and 4.5432, respectively, as shown in Table.4. Compared to the theoretical value, the maximum measurement error was approximately less than 4 %.

Table. 4 The Measured Errors of the topological charges

Theoretical value	2.500	3.500	4.500
Average value	2.549	3.632	4.452
Error [%]	2.0	3.8	1.1

3.4. Measurement error in wavefront of Gaussian beam

The measurement accuracy of VB phase measurement is affected by fluctuations in the Gaussian beam of the reference light (i.e., the wavefront of the light collimated from the laser). The tilt with respect to the reference plane was detected directly as the overall tilt of the phase distribution.

To investigate the accuracy due to the wavefront error, we measured the interference between the Gaussian beam used as the reference and a similar Gaussian beam reflected from the SLM (the surface of the SLM was set flat without hologram). The phase profile fluctuation and flatness obtained from this system were used as indicators of the wavefront error in the VB measurement.

Ten consecutive measurements were conducted in the same manner, and the correspondence with the mean value of the phase distribution was obtained, as shown in Fig.3.17(a). An ideal plane of the mean distribution of the measured wavefront (shown in Fig. 3.17(a)) was fitted using the least-squares method, as shown in Fig.3.17 (b), and the difference between the measured and fitting distributions was calculated, as shown in Fig. 3.17 (c). The flatness of the wavefront was 0.06 rad according to the root-mean-square (RMS) of Fig.3.17 (c), revealing the potential wavefront error in the spatial propagation of the VB.

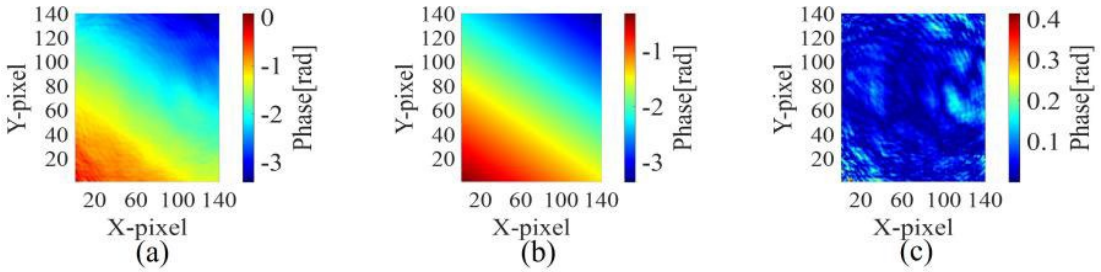

Fig.3.17. Average value of phase distribution of Gaussian beam with 10 measurements. (a) The measured phase distribution. (b). The fitting result of phase distribution. (c). The phase different between the measured phase distribution and fitting result.

3.5. Summary

In this section, the VB with the fractional and integer order were successfully generated by a SLM and corresponding the holograms of phase mapping of VB were designed by computer. The phase distributions of VB were directly obtained via FFT algorithm. To determine the topological charge of VB, the phase unwrapping method based on polar coordinates was proposed and the effect of phase singularity can be effectively eliminated by means of the measured intensity distribution of VB. Consequently, the maximum phase variation of VB without the phase singularity was extracted to estimate the topological. For 11 measurements in different radius, the maximum measurement error was approximately within 4%. According the phase distribution of wavefront of Gaussian beam, it shows the tiny fluctuation in wavefront in the free space propagation and further reveals the potential measurement error in the reference wave.

4. Conclusion

In this thesis, we introduced the concept of vortex beam and some applications with VB in many fields in detail. The VB is the one of particular solution for maxwell's equations under the condition of paraxial approximation. In the condition of paraxial approximation, it can be described by the scalar Helmholtz equation as well. Owing to possess the spiral wavefront, this type of light beam is called as the VB. The common light with a spiral phase in experiment has LG beam and BS beam, and so on. Specially, the BS beam generally is modified by the Gaussian function to generate the BG beam. Owing to similar property of non-diffraction, BG-beam has been widely employed in optical communication. The spiral phase structure yields a phase singularity with the undefined amplitude and the amplitude of zero. Moreover, each photon of VB possesses the OAM that has been demonstrated. Considering the unique property of OAM, many applications using the VB has been developed in many fields, such as the optical tweezers and optical communication and so on. Hence, the phase measurement of VB is gradually important to the development of application and VB quality. Some methods of the measurement and estimation of phase and topological charge of VB have been proposed. However, these methods have the obvious disadvantage due to the complex configuration and the stringent experimental environment.

In this thesis, a SPM method was proposed to achieve the optical vortex phase measurement purpose. The SPM interferometry was modified by the Michelson interferometry via a mirror attached to a PZT with a signal generator. The VB was generated by a SLM and the interference signal with the sinusoidal modulation can be obtained by the discrete signal processing via the recorded interference fringes over 8

periods. Moreover, the wrapped phase distribution of VB can be directly obtained by means of the FFT algorithm. Then the phase unwrapping method of VB was proposed to estimate quantitatively the topological charge and a method based on the measured intensity of VB was used for reducing the effect of phase singularity in measurement result. Consequently, the topological charge with the fractional and integer was succeeded in quantitative estimation. By means of repeated measurements in 11 measurements, the measurement results were evaluated by the average value and STD of measurements. Moreover, the maximum measurement error was determined to be approximately 4%, which reveals the phase measurement of VB has the high measurement and stability. Finally, the fluctuation of wavefront of Gaussian beam reveals the potential measurement error in reference wave after the free space propagation.

5. Future research.

With the development of optical detection technique on the rise gradually, optical detection technique has been employed in wide range of fields. For example, the optical coherence tomography based the property of the low coherent light has been widely employed in medicine field and the quality inspection of sample. With the development of life sciences, optical detection technique is gradually to be significant.

Nevertheless, these methods based on the interferometric technique has high sensitivity on the low-frequency noise and it has effect on the measurement accuracy. To solve this issue, prof. Suzuki proposed the feedback method to obtain the stable interference signal and reduce the effect of noise effectively. Consequently, the step height of gauge-block was measured precisely. Nevertheless, the common light beam such as Gaussian beam through the scattering medium lead to the scattered light.

The VB as a detection light has been employed in measurement of the vibration of object due to the high stability and antijamming capability. Nevertheless, the effect of low-frequency noise is difficult to be ignored in measurement result. In the application of OCT, the dispersion compensation algorithm has been adopted in improved the quality of image. By the unceasing phase modulation using the Hilbert transform and image evaluation function as the standard of feedback, the high quality of image with high contrast can be obtained. In the future research, the VB as a detection is used for measuring the step height of gauge-block under the condition of the VB through the scattering medium. By means of the discrete signal processing with the phase modulation algorithm conducted by SLM, the ideal interference fringe can be acquired. The corresponding phase is obtained by the spatial carrier frequency algorithm via FFT.

Reference

1. Heckenberg N R, McDuff R, Smith C P, et al. Generation of optical phase singularities by computer-generated holograms[J]. Optics letters, 1992, 17(3): 221-223.
2. Bazhenov V Y, Vasnetsov M V, Soskin M S. Laser beams with screw dislocations in their wavefronts[J]. Jetp Lett, 1990, 52(8): 429-431.
3. Zernike F. The concept of degree of coherence and its application to optical problems[J]. Physica, 1938, 5(8): 785-795.
4. Nye J F, Berry M V. Dislocations in wave trains[J]. Proceedings of the Royal Society of London. A. Mathematical and Physical Sciences, 1974, 336(1605): 165-190.
5. Gori F, Ramírez-Sánchez V, Santarsiero M, et al. On genuine cross-spectral density matrices[J]. Journal of Optics A: Pure and Applied Optics, 2009, 11(8): 085706.
6. Coullet P, Gil L, Rocca F. Optical vortices[J]. Optics Communications, 1989, 73(5): 403-408.
7. Shen Y, Wang X, Xie Z, et al. Optical vortices 30 years on: OAM manipulation from topological charge to multiple singularities[J]. Light: Science & Applications, 2019, 8(1): 90.
8. Gahagan K T, Swartzlander G A J. Optical vortex trapping of particles[J]. Optics Letters, 1996, 21(11): 827-829.
9. Nakaya S, Kozawa Y, Uesugi Y, et al. Optical Trapping of Low Refractive Index Particles by Dual Vortex Beams[C]//CLEO: Science and Innovations. Optica Publishing Group, 2021: SM4I. 3.
10. Simpson N B, Dholakia K, Allen L, et al. Mechanical equivalence of spin and orbital angular momentum of light: an optical spanner[J]. Optics letters, 1997, 22(1): 52-54.
11. Zhang H, Li J, Cheng K, et al. Trapping two types of particles using a focused partially coherent circular edge dislocations beam[J]. Optics & Laser Technology, 2017, 97: 191-197.
12. Yang C, Lan Y, Jiang X, et al. Beam-holding property analysis of the perfect optical vortex beam

transmitting in atmospheric turbulence[J]. Optics Communications, 2020, 472: 125879.

13. Čelechovský R, Bouchal Z. Optical implementation of the vortex information channel[J]. New Journal of Physics, 2007, 9(9): 328.
14. Zhang Q, Pang C, Yang L, et al. Parallel Coded Optical Vortex Beam Free-Space Communication Based on Single-Photon Detection[J]. IEEE Photonics Journal, 2022, 14(3): 1-6.
15. Ruffato G, Massari M, Romanato F. Multiplication, and division of the orbital angular momentum of light with diffractive transformation optics[J]. Light: Science & Applications, 2019, 8(1): 113.
16. Tang S, Cai T, Wang G M, et al. High-efficiency dual-modes vortex beam generator with polarization-dependent transmission and reflection properties[J]. Scientific reports, 2018, 8(1): 6422.
17. Li C, Liu S, Wang W, et al. Recent research on stimulated emission depletion microscopy for reducing photobleaching[J]. Journal of microscopy, 2018, 271(1): 4-16.
18. Grier D G. A revolution in optical manipulation[J]. nature, 2003, 424(6950): 810-816.
19. Cui S, Xu B, Luo S, et al. Determining topological charge based on an improved Fizeau interferometer[J]. Optics express, 2019, 27(9): 12774-12779.
20. de Araujo L E E, Anderson M E. Measuring vortex charge with a triangular aperture[J]. Optics letters, 2011, 36(6): 787-789.
21. Kumar P, Nishchal N K. Modified Mach–Zehnder interferometer for determining the high-order topological charge of Laguerre–Gaussian vortex beams[J]. JOSA A, 2019, 36(8): 1447-1455.
22. Hu X, Gezhi Z, Sasaki O, et al. Topological charge measurement of vortex beams by phase-shifting digital hologram technology[J]. Applied Optics, 2018, 57(35): 10300-10304.
23. Guo J, Zheng S, Zhou K, et al. Measurement of real phase distribution of a vortex beam propagating in free space based on an improved heterodyne interferometer[J]. Applied Physics Letters, 2021, 119(2): 023504.

24. Pu H, Sasaki O, Suzuki T, et al. Measurements of phase distributions of optical vortices based on the sinusoidal phase modulation method[J]. Optics Continuum, 2022, 1(11): 2287-2297.

25. Wei B, Hu W, Ming Y, et al. Generating switchable and reconfigurable optical vortices via photopatterning of liquid crystals[J]. Advanced Materials, 2014, 26(10): 1590-1595.

26. Lloyd S M, Babiker M, Thirunavukkarasu G, et al. Electron vortices: Beams with orbital angular momentum[J]. Reviews of Modern Physics, 2017, 89(3): 035004.

27. Sztul H. Optical vortices: angular momentum of light, energy propagation, and imaging[M]. City University of New York, 2008.

28. Snyder A W, Love J D. Optical waveguide theory[M]. London: Chapman and hall, 1983.

29. Mair A, Vaziri A, Weihs G, et al. Entanglement of the orbital angular momentum states of photons[J]. Nature, 2001, 412(6844): 313-316.

30. Allen L, Beijersbergen M W, Spreeuw R J C, et al. Orbital angular momentum of light and the transformation of Laguerre-Gaussian laser modes[J]. Physical review A, 1992, 45(11): 8185.

31. Guo Z, Wang Z, Dedo M I, et al. The orbital angular momentum encoding system with radial indices of Laguerre–Gaussian beam[J]. IEEE Photonics Journal, 2018, 10(5): 1-11.

32. Durnin J, Miceli Jr J J. Nondiffracting beams[J]. Optics News, 1987, 13(12): 27-27.

33. Rosales-Guzmán C, Forbes A. How to shape light with spatial light modulators[C]. Society of Photo-Optical Instrumentation Engineers (SPIE), 2017.

34. Zhang K, Wang Y, Yuan Y, et al. A review of orbital angular momentum vortex beams generation: from traditional methods to metasurfaces[J]. Applied sciences, 2020, 10(3): 1015.

35. Fickler R, Campbell G, Buchler B, et al. Quantum entanglement of angular momentum states with quantum numbers up to 10,010[J]. Proceedings of the National Academy of Sciences, 2016, 113(48): 13642-13647.

36. Kotlyar V V, Almazov A A, Khonina S N, et al. Generation of phase singularity through diffracting

a plane or Gaussian beam by a spiral phase plate[J]. JOSA A, 2005, 22(5): 849-861.

37. Sueda K, Miyaji G, Miyanaga N, et al. Laguerre-Gaussian beam generated with a multilevel spiral phase plate for high intensity laser pulses[J]. Optics express, 2004, 12(15): 3548-3553.

38. Carpentier A V, Michinel H, Salgueiro J R, et al. Making optical vortices with computer-generated holograms[J]. American Journal of Physics, 2008, 76(10): 916-921.

39. Padgett M, Courtial J, Allen L. Light's orbital angular momentum[J]. Physics today, 2004, 57(5): 35-40.

40. Szatkowski M, Masajada J, Augustyniak I, et al. Generation of composite vortex beams by independent Spatial Light Modulator pixel addressing[J]. Optics Communications, 2020, 463: 125341.

41. Fickler R, Lapkiewicz R, Plick W N, et al. Quantum entanglement of high angular momenta[J]. Science, 2012, 338(6107): 640-643.

42. Marrucci L, Manzo C, Paparo D. Optical spin-to-orbital angular momentum conversion in inhomogeneous anisotropic media[J]. Physical review letters, 2006, 96(16): 163905.

43. Marrucci L, Karimi E, Slussarenko S, et al. Spin-to-orbital conversion of the angular momentum of light and its classical and quantum applications[J]. Journal of Optics, 2011, 13(6): 064001.

44. Ashkin A. Acceleration and trapping of particles by radiation pressure[J]. Physical review letters, 1970, 24(4): 156.

45. H. He, M. E. J. Friese, N. R. Heckenberg and H. Rubinsztein-Dunlop,"Direct observation of transfer of angular momentum to absorptive particles from a laser beam with a phase singularity," Phys. Rev. Lett. 75(5), 826-829 (1995).

46. Courtial J, Dholakia K, Allen L, et al. Second-harmonic generation and the conservation of orbital angular momentum with high-order Laguerre-Gaussian modes[J]. Physical Review A, 1997, 56(5): 4193.

47. Garcés-Chávez V, McGloin D, Padgett M J, et al. Observation of the transfer of the local angular

momentum density of a multiringed light beam to an optically trapped particle[J]. Physical review letters, 2003, 91(9): 093602.

48. Lee W M, Yuan X C, Cheong W C. Optical vortex beam shaping by use of highly efficient irregular spiral phase plates for optical micromanipulation[J]. Optics letters, 2004, 29(15): 1796-1798.
49. Curtis J E, Koss B A, Grier D G. Dynamic holographic optical tweezers[J]. Optics communications, 2002, 207(1-6): 169-175.
50. Schmiegelow C T, Larotonda M A. Multiplexing photons with a binary division strategy[J]. Applied Physics B, 2014, 116(2): 447-454.
51. Hell S W, Wichmann J. Breaking the diffraction resolution limit by stimulated emission: stimulated-emission-depletion fluorescence microscopy[J]. Optics letters, 1994, 19(11): 780-782.
52. Lauterbach M A, Guillon M, Soltani A, et al. STED microscope with spiral phase contrast[J]. Scientific Reports, 2013, 3(1): 1-5.
53. Galiani S, Harke B, Vicidomini G, et al. Strategies to maximize the performance of a STED microscope[J]. Optics express, 2012, 20(7): 7362-7374.
54. Tian N, Fu L, Gu M. Resolution, and contrast enhancement of subtractive second harmonic generation microscopy with a circularly polarized vortex beam[J]. Scientific Reports, 2015, 5(1): 1-8.
55. Willner A E, Wang J, Huang H. A different angle on light communications[J]. Science, 2012, 337(6095): 655-656.
56. Lei T, Zhang M, Li Y, et al. Massive individual orbital angular momentum channels for multiplexing enabled by Dammann gratings[J]. Light: Science & Applications, 2015, 4(3): e257-e257.
57. Gibson G, Courtial J, Padgett M J, et al. Free-space information transfer using light beams carrying orbital angular momentum[J]. Optics express, 2004, 12(22): 5448-5456.

58. Krenn M, Fickler R, Fink M, et al. Communication with spatially modulated light through turbulent air across Vienna[J]. New Journal of Physics, 2014, 16(11): 113028.

59. Ishikawa K, Yatabe K, Ikeda Y, et al. Interferometric imaging of acoustical phenomena using high speed polarization camera and 4-step parallel phase-shifting technique[C]//Selected Papers from the 31st International Congress on High-Speed Imaging and Photonics. SPIE, 2017, 10328: 93-99.

60. Yim N B, Eom C I, Kim S W. Dual mode phase measurement for optical heterodyne interferometry[J]. Measurement Science and Technology, 2000, 11(8): 1131.

61. Sasaki O, Okazaki H. Analysis of measurement accuracy in sinusoidal phase modulating interferometry[J]. Applied optics, 1986, 25(18): 3152-3158.

62. Sasaki O, Okazaki H. Sinusoidal phase modulating interferometry for surface profile measurement[J]. Applied optics, 1986, 25(18): 3137-3140.

Acknowledgement

I am deeply grateful to all the individuals who have supported me throughout my PhD journey. Their guidance, encouragement and inspiration have been invaluable to me, and I could not have completed this thesis without their help.

First and foremost, I would like to express my sincere appreciation to my advisor, Professor Choi, for his tremendous guidance, support, and encouragement throughout my PhD studies. His valuable suggestions, constructive criticisms, and unwavering belief in me have been a source of inspiration, and I am deeply grateful for his mentorship.

I am also deeply grateful to Professor Suzuki for introducing me to the academic world and providing me with opportunities to expand my knowledge and skills. I am grateful for his encouragement, guidance, and support, and I hope that I can repay his kindness in the future.

I would also like to extend my heartfelt thanks to Professor Sasaki for his kindness and care in my daily life. His generosity and support have been a source of comfort and encouragement, and I will always be grateful for his influence in my life.

I am also grateful to all my colleagues, classmates and friends for their friendship and support throughout my PhD journey. I have learned so much from them and I am grateful for their contributions to my academic and personal growth.

Finally, I would like to express my sincere gratitude to my family for their unwavering love, support, and encouragement throughout my life. Their sacrifices and dedication have been a source of inspiration and motivation, and I could not have accomplished this without their support.

This thesis is a testament to the hard work and dedication of all those who have supported me throughout my PhD journey. I am deeply grateful for their contributions and I hope that this work will make a meaningful contribution to the field.